J. Chem. Soc., Faraday Trans. 1, 1988, **84**(11), 3821–3849

Some New Developments in Solid-state Nuclear Magnetic Resonance Spectroscopic Studies of Lipids and Biological Membranes, including the Effects of Cholesterol in Model and Natural Systems

Jeffrey Forbes, John Bowers, Xi Shan, Liam Moran and Eric Oldfield*
School of Chemical Sciences, University of Illinois at Urbana–Champaign, 505 South Mathews Avenue, Urbana, Illinois 61801, U.S.A.

Mario A. Moscarello
Department of Biochemistry, Hospital for Sick Children, University of Toronto, Canada M5S 1A8

High-field proton magic-angle sample-spinning (MAS) nuclear magnetic resonance (NMR) spectroscopy is shown to yield high-resolution ^1H spectra of smectic, nematic and hexagonal-II phase lipids, from which isotropic chemical shifts, order parameters and relaxation times (T_1, $T_{1\rho}$ and T_2) can be determined. Such experiments are possible because of the special form of the dipolar Hamiltonian in such systems. Resolution is about the same as that obtained with sonicated systems, using conventional NMR techniques. We also show that ^{13}C MAS NMR spectra, of both fluid and solid phases, are even better resolved, and in some cases resonances can be observed in MAS NMR spectra which are not observable in sonicated systems. For example, essentially all of the carbon atoms in cholesterol (CHOL) can be readily detected and assigned in a lecithin–CHOL bilayer, using MAS, while few can be seen in sonicated bilayers. This leads directly to the observation of cholesterol in intact biological membranes, such as human myelin, where over 50 peaks can be observed, and *ca.* 40 of these resonances can be assigned to specific, single-carbon-atom sites in the membrane. In addition, a number of experiments with massively deuterated lipids are reported. Combination of cross-polarization techniques with MAS, and difference spectroscopy, leads to the observation of essentially pure sterol spectra (in the presence of lipid) and pure lipid spectra (in the presence of CHOL). Analysis of chemical-shift results indicates a substantial deshielding of chain carbon atom resonances caused by the presence of CHOL, due presumably to increased *trans* chain segments, an effect mirrored in variable temperature spectra of human myelin, and in goldfish myelin. Taken together, these results suggest a resurgence in NMR studies of membranes may soon occur.

Early wide-line studies of lipids and related systems showed that useful information on dynamic structure could be obtained,[1,2] however, spectra were of low resolution owing to the dominance of static dipole–dipole interactions. Chapman and Penkett[3] reported that ultrasonic dispersal of lipids enabled chemically shifted high-resolution spectra to be obtained, due to a reduction in particle size, and an overall increase in effective rotational correlation time, τ_c. Chapman and Penkett showed that cholesterol caused a decrease in mobility of lipid hydrocarbon chains owing to the bulky nature of the sterol nucleus, and later Chapman *et al.* extended such studies to investigation of biological membranes themselves, such as those of erythrocyte ghosts[4] and myelin membranes from brain.[5] Other workers showed, however, that sonication could cause a variety of

chemical and other ultrastructural changes,[6,7] and in addition, the difficulty in dissecting particle size from internal motional effects in bilayers was noted.[8,9] Thus, it became apparent that sonic disruption of lipids or biomembranes had a number of potentially undesirable features. We have therefore attempted to devise a number of new approaches to the investigation of membrane structure, using NMR methods, which avoid the necessity of sonic dispersal of the membrane system of interest.

In the early 1970s the origin of the line broadening in the ^{1}H NMR spectra of membranes was unclear, with magnetic field gradients, and diffusion through said gradients, being thought to contribute to the apparently field-dependent linewidths observed. However, Tiddy,[10] Chan *et al.*[11] and ourselves[12] showed that spectra were in fact field-independent, strongly implicating a purely dipolar origin for the experimental linewidths seen. We thus reasoned that ^{1}H 'magic-angle' sample-spinning (MAS, ≡ 'magic-angle' rotation, MAR) might be effective in line narrowing, and we reported on preliminary results at 60 MHz, with Doscočilová and Schneider, in 1972.[13] Since resolution was not spectacular, we therefore also investigated ^{13}C NMR of a variety of unsonicated lipids and biological membranes, again with only moderately promising results.[14,15] Finally, we embarked upon a programme of ^{2}H NMR studies of lipids and membranes,[16,17] an area which over the past 15 years has shown considerable growth, and has yielded a wealth of information on the static and dynamic structure of membranes [see ref. (18) and references cited therein]. Why then, try to improve on ^{2}H NMR?

One drawback of the ^{2}H NMR method is that it requires chemical synthesis, a generally difficult, expensive and time-consuming procedure. We thus decided recently to reinvestigate the same types of system studied in the late 1960s and early 1970s using basically the same types of technique we used then, ^{13}C NMR and ^{1}H MAS, but taking advantage of the major technological developments that have occurred in the past 10–20 years, *i.e.* by using very-high-field (11.7 T) magnets and Fourier-transform methods. As we show in this paper, and in preliminary form elsewhere,[19,20] high-field ^{1}H MAS yields very-high-resolution NMR spectra of lipids and membranes, due to the special form of the dipolar Hamiltonian, $\mathscr{H}_d$, ^{1}H MAS NMR spectra being essentially indistinguishable from those of similar sonicated samples. Relaxation times T_1, T_2 and $T_{1\rho}$ can be studied, as can spin-diffusion, for each resolved individual site in the membrane; two-dimensional NMR techniques can also be profitably applied. We also show, as expected based on the early work of others,[21–23] that ^{13}C MAS NMR results are even more promising, especially since in some situations many ^{13}C sites in unsonicated membranes can be observed which are 'invisible' in sonicated systems.[19,24] This leads to the first realization of a 20 year-old goal: the first observation of numerous, resolved, single-carbon-atom sites in biologial membranes themselves, such as the red cell ghost, and myelin, from different species. Overall, our results appear extremely promising, and represent by far the most highly resolved and informative spectra of any membrane system obtained to date.

Experimental

NMR Spectroscopy

All ^{1}H and ^{13}C NMR spectra were obtained on 'home-built' NMR spectrometers, which operate at 50 and 500 MHz for ^{1}H, using either a Nalorac (Martinez, CA) 4.0 in† bore 1.18 T magnet, or with an Oxford Instruments (Osney Mead, U.K.) 2 in bore, 11.7 T superconducting solenoid, together with Nicolet (Madison, WI) model 1280 computer systems, Henry Radio (Los Angeles, CA) model 1002 radiofrequency amplifiers, Amplifier Research (Souderton, PA) model 200L radiofrequency amplifiers, and either

† in = 2.54×10^{-2} m.

Doty Scientific (Columbia, S.C.) MAS NMR probes (7 mm at 1.18 T, 5 mm at 11.7 T), or a 5 mm multinuclear solution NMR probe (Cryomagnet Systems, Indianapolis, IN). For ^1H MAS experiments the 90° pulse widths were 8 μs, and spinning rates were *ca.* 2.4–3.5 kHz. For sonicated samples the ^1H 90° pulse width was 12 μs. For ^{13}C MAS, dipolar decoupled (40 W ^1H power) Bloch decays were recorded, using 9 μs ^{13}C 90° pulse widths. ^{13}C CP-MAS spectra were recorded using mix times of either 5 or 10 ms; other conditions were as stated above for ^{13}C MAS. For ^{13}C NMR of sonicated samples, 10 μs 90° pulse widths were used, together with Waltz-16 proton decoupling (gated at 0.5 and 5 W), to ensure full decoupling and a nuclear Overhauser effect, but without appreciable sample heating. Temperature was adjusted *via* a gas-flow cryostat, and values reported were gas-flow temperatures monitored with a Doric (San Diego, CA) Trendicator, with the thermocouple placed near the sample. All spectra were referenced to an external standard of tetramethylsilane, and high-frequency, low-field, deshielded, paramagnetic shifts are denoted as positive (IUPAC δ scale).

Lipid Samples

Sodium decanoate was prepared by titrating decanoic acid (Sigma Chemical Corporation, St. Louis, MO) with reagent-grade NaOH (J. T. Baker, Phillipsburg, NJ) in EtOH, to a phenolphthalein endpoint, followed by recrystallization from EtOH, at −20 °C. The product was dried at 100 °C for 24 h. Decanol was from Aldrich (Milwaukee, WI) and was used as received. Egg-yolk lecithin (EYL) was obtained from Lipid Products (South Nutfield, Surrey) and was used without further purification. 1,2-Dimyristoyl and 1,2-dipalmitoyl-*sn*-glycero-3-phosphocholine (DPMC; DPPC) were from Sigma. [1,2-$^2H_{54}$]dimyristoyl and [1,2-$^2H_{62}$]dipalmitoyl-*sn*-glycero-3-phosphocholine ([$^2H_{54}$]-DPMC and [$^2H_{62}$]-DPPC) and *N*-Me[$^2H_9$]-1,2-dipalmitoyl-*sn*-glycero-3-phosphocholine ([$^2H_9$]-DPPC) were from Avanti Polar Lipids, Inc. (Birmingham, AL). 1,2-dioleoyl-*sn*-glycero-3-phosphoethanolamine (DOPE) and beef-brain galactocerebroside were from Sigma. *N*-(4-methoxybenzylidene)-4′-n-butylaniline (MBBA) and cholesterol were from Aldrich. Cholesterol was recrystallized three times from EtOH before use. All other steroids (stigmasterol, desmosterol and lanosterol) were from Steraloids, Inc. (Wilton, NH), and were used as received.

The sodium decanoate–decanol–water liquid-crystalline phase was prepared by combining the appropriate amounts of the components, followed by extensive homogenization at *ca.* 70 °C. EYL samples were prepared by addition of the appropriate amount of '100%' D_2O (Sigma) to dried EYL, and either dispersing by hand, or for 3 × 6 min periods of sonication using a Heat Systems-Ultrasonics (Plainview, NY) ultrasonicator. Sample temperature was kept low by having the sonicating vial surrounded by ice, and by agitating the sample for 2 min in the ice between sonic bursts. EYL–CHOL samples were prepared by co-dissolving the appropriate amounts of EYL and CHOL in $CHCl_3$, removing the solvent under an N_2 stream at *ca.* 40 °C, followed by evacuation over P_4O_{10} for 24 h. The samples were then hydrated to the appropriate level (50 wt% lipid for an unsonicated dispersion, 10 wt% for a sonicated dispersion) and dispersed, basically as described above for EYL. Other pure lipid or lipid–sterol hand dispersions were all prepared using a basically identical protocol. Sample purity was monitored periodically *via* thin-layer chromatography on Eastman Chromagram silica-gel sheets no. 6061 (Eastman Kodak, Rochester, N.Y.) using a $CHCl_3$:MeOH:7 mol dm^{-3} NH_4OH (230:90:15, v/v) solvent system, with molybdenum blue as a visualizing agent.[25,26]

Human myelin was isolated from an autopsy sample, basically as described elsewhere.[27] Goldfish were obtained from a local, commercial pisciculturalist, and goldfish myelin was also isolated basically as described in ref. (27).

Results and Discussion

Proton MAS Yields High-resolution Spectra of Smectic Liquid Crystals

Conventional wisdom, supported by our early work, strongly indicated that ^{1}H spinning experiments on phospholipids should not be very successful, since the criterion to achieve complete narrowing was thought to be that the rotation rate, ν_r, must be greater than the dipolar width, as discussed by Maricq and Waugh.[28] While this is true, it can also be misleading in the sense that to be 'successful', all that is really required is that the Hamiltonian describing the interaction commutes with itself at different rotor orientations, *i.e.* if the broad static spectrum breaks up into spinning sidebands at low spinning speeds, then a 'useful' high-resolution spectrum (plus spinning sidebands) can be obtained, even in the limit that $\nu_r \ll W$, where W is the overall spectral breadth. This is now well appreciated for 'inhomogeneous' interactions, such as the chemical shift and first-order quadrupolar interaction, but also applies in the case of certain dipolar interactions, as in the case of a linear chain of spins (*e.g.* ^{19}F in fluoroapatite).[29]

We show in fig. 1 (*a*) and (*b*) the 50.6 MHz ^{1}H MAS NMR spectra of a smectic liquid-crystalline mesophase comprised of 38.9% decanol, 30.1% sodium decanoate and 31% ^2H_2O. This mesophase is of a type that yields a broad (*ca.* 10 kHz) so-called super-Lorentzian line in the non-spinning state, as first observed by Lawson and Flautt,[30] but even on slow MAS [820 Hz, fig. 1 (*a*)], we find that the spectrum breaks up into a large number (> 30) of spinning sidebands, each of which is quite narrow (*ca.* 120 Hz). On more rapid spinning, fig. 1 (*b*), the sidebands move away from the central peak, and some fine structure, better seen in the MAS NMR spectrum of unsonicated DMPC, fig. 2, becomes apparent.

The observation of such high-resolution ^{1}H MAS NMR spectra are rather surprising, since the static dipolar Hamiltonian

$$\sum_{i<j} D_{ij}(\phi)\,(3I_{zi}I_{zj} - \boldsymbol{I}_i \cdot \boldsymbol{I}_j) \tag{1}$$

does not in general commute with itself at different rotor orientations, ϕ. However, in the smectic liquid-crystalline phase, intermolecular dipole–dipole interactions are averaged by fast lateral diffusion, while fast axial rotation reduces the intramolecular dipole–dipole interaction, and causes the angular dependence of the Hamiltonian to be the same for all proton pairs.[31–33] Thus the dipolar interaction is scaled by $P_2(\cos\theta)$, where θ is the angle between the director axis and H_0, such that

$$D_{ij} = \tfrac{1}{2}(3\cos^2\theta - 1)\,D_{ij}^{\circ} \tag{2}$$

and the Hamiltonian becomes

$$\tfrac{1}{2}(3\cos^2\theta - 1) \sum_{i<j} D_{ij}^{\circ}[3I_{zi}I_{zj} - \boldsymbol{I}_i \cdot \boldsymbol{I}_j] \tag{3}$$

which under MAS commutes with itself at different rotor orientations, ϕ. The result is that the dipole–dipole interaction is inhomogeneous, in the sense that line narrowing, and the generation of sharp spinning sidebands, is achieved at sample rotation rates much slower than the static spectral breadth.

Interestingly, the envelope of the spinning sidebands in the slow-spin spectrum shown in fig. 1 (*a*) is very close to the theoretical 'super-Lorentzian' lineshape superimposed on the experimental MAS NMR spectrum, given by:[31]

$$L(\nu - \nu_0) = \int_0^1 |3\cos^2\theta - 1|^{-1} \times f[(\nu - \nu_0)/|3\cos^2\theta - 1|]\,\mathrm{d}\cos\theta \tag{4}$$

the lineshape being calculated for an assumed Gaussian shape of $f(x)$, as shown in fig. 1 (*a*).

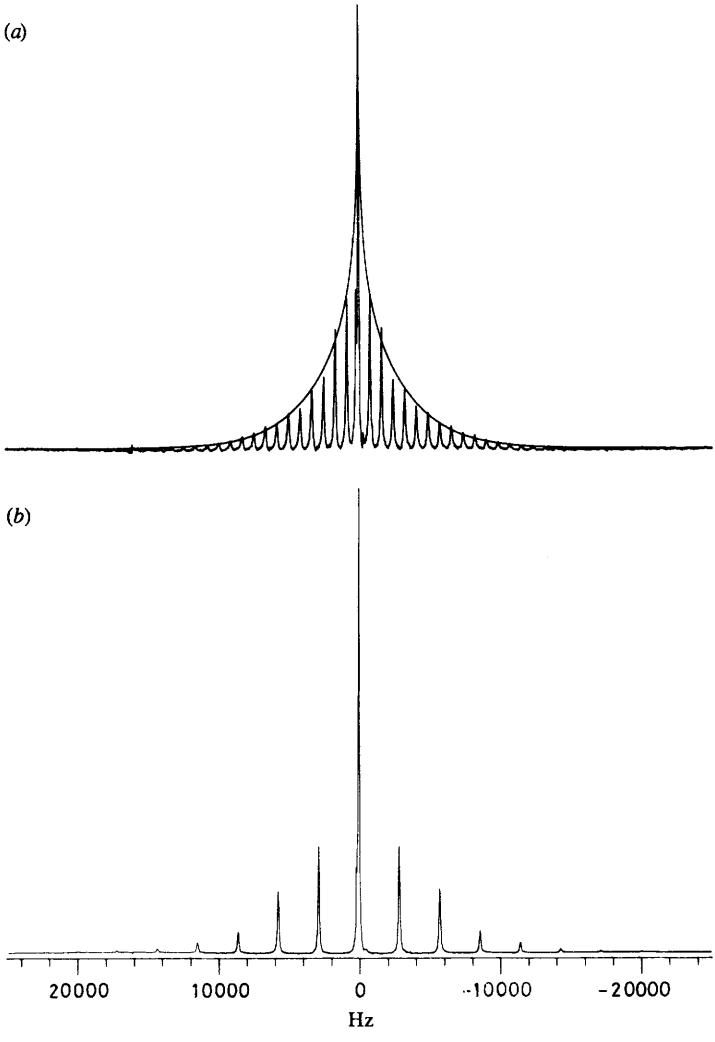

Fig. 1. 50.6 MHz ^{1}H Fourier-transform MAS NMR spectra of decanol (38.9%)–sodium decanoate (30.1%)–D_2O (31.0%) at 21 °C. (*a*) 0.82 kHz spinning speed. (*b*) 2.86 kHz spinning speed. Recycle times of 5 s, 32 acquisitions and 10 Hz exponential line-broadening were utilized in both spectra. Superimposed on the 0.82 kHz MAS NMR spectrum is the 'super-Lorentzian' lineshape calculated using eqn (4) with an assumed Gaussian lineshape function, $f(x) = \exp(-\pi x^2)$.

Similar breakdown of the static lineshape into numerous sharp spinning sidebands has been observed for all of the other smectic liquid-crystalline phase lipids we have investigated, including egg lecithin, egg phosphatidylcholine, beef-brain sphingomyelin, beef-heart cardiolipin, potassium oleate–water mixtures, phosphatidyl inositol, dioleoyl phosphatidylcholine and DPPC, and similar results are to be expected in other liquid crystals in which fast lateral diffusion averages intermolecular dipole–dipole interactions, and fast axial rotation causes the special symmetry properties outlined above.

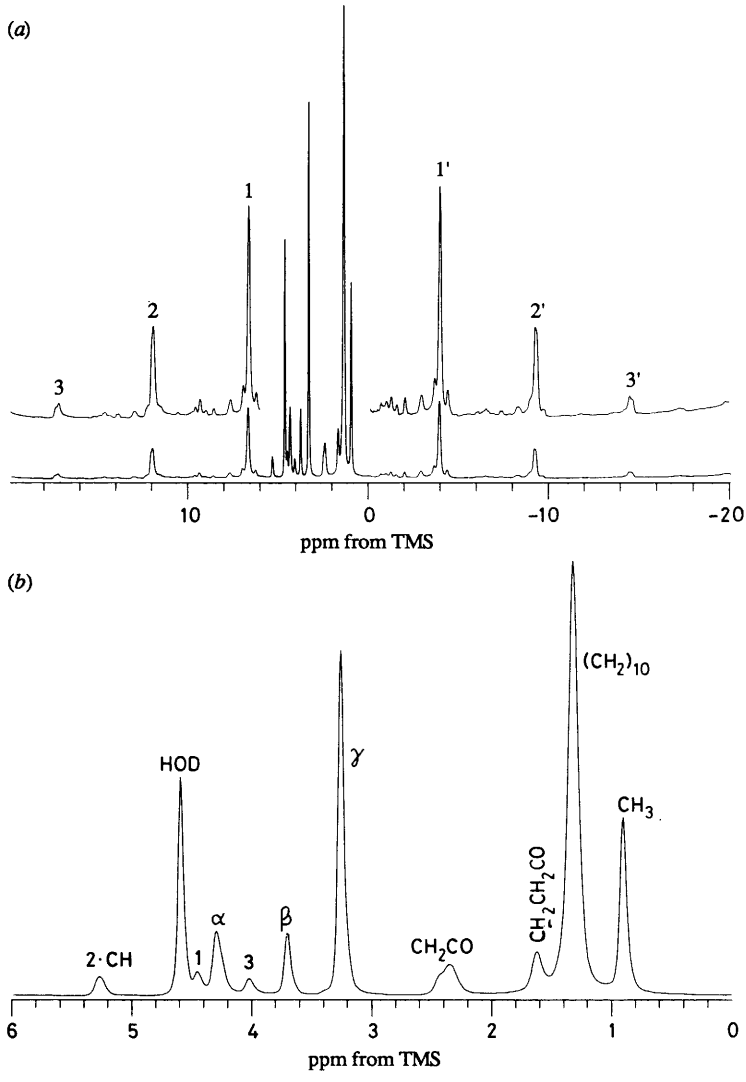

Fig. 2. 500 MHz ^{1}H Fourier-transform MAS NMR spectrum of 1,2-dimyristoyl-*sn*-glycero-3-phosphocholine (DMPC)–^2H_2O (50 wt%) at 36 °C. (*a*) 2.7 kHz spectrum, showing spinning sidebands (1, 2, 3, 1′, 2′, 3′). (*b*) Expansion of the centreband region in (*a*). A recycle time of 8 s, 32 acquisitions and a 5 Hz exponential line-broadening were utilized.

Order Parameters may be deduced from some Proton MAS Spectra

We show in fig. 2 the 500 MHz ^{1}H MAS NMR spectrum of a 50 wt% hand dispersion of DMPC in D_2O, at 36 °C. The spectrum shown clearly consists of a rather crowded, central, high-resolution part, shown expanded in fig. 2(*b*), together with three more or less well resolved (or observable) spinning sidebands, noted 1 (1′), 2 (2′) and 3 (3′) in fig. 2(*a*). The assignments of the major features in the expanded high-resolution part of the spectrum [fig. 2(*b*)] follow readily from the literature assignments,[34] and are un-noteworthy.

What is more interesting is that the spectral intensities of each of the major assignable

features in the high-resolution (central), portion of the spectrum are at variance with their theoretical intensity ratios. For example, the chain terminal methyl intensity (at 0.91 ppm from tetramethylsilane, TMS), is *ca.* 37% that of the chain $(CH_2)_{10}$ resonance (at 1.33 ppm), compared with a theoretical 15% value (3/20). The origin of this effect is clearly due to the presence of additional $(CH_2)_{10}$ intensity in the spinning sidebands. When account is taken of the total (centreband plus sideband) intensities, then good ($\pm 10\%$) agreement between the experimental and theoretical intensity ratios is obtained.[20]

Fig. 2(*a*) clearly shows that the SSB 'spectra' are quite distorted relative to the centreband spectrum, fig. 2(*b*). We believe this interesting effect must arise from the different scalings of the overall dipolar interactions, or more specifically, must be due to the fact that the individual dipolar interactions, or second moments, of the individual groups, are scaled by an order parameter, S_{dip}, the dipolar (pseudo) order parameter, owing to the different amounts of motional averaging occurring in each part of the lipid molecule.

This follows since, as shown above, the dipolar interaction is scaled by the term, $P_2(\cos\theta)$, so the residual second moment of a given resonance (M_{2r}) is also dependent upon θ, the angle between the bilayer normal and the static magnetic field, H_0, and, as Bloom has shown,

$$M_{2r}(\theta) = M_{2r}(0)\,[P_2(\cos\theta)]^2. \tag{5}$$

The expression for M_{2r} can be conveniently expressed for the alkyl chains in terms of a set of dipolar pseudo-order parameters, S_{jk}, defined by:[33]

$$S_{jk} = (r_{jk}^{\circ})^3 \langle P_2(\cos\chi_{jk})/r_{jk} \rangle \tag{6}$$

where r_{jk} is the instantaneous distance between spins j and k, r_{jk}° is the corresponding distance in the all-*trans* conformation, and χ_{jk} is the angle between r_{jk} and the director axis. For alkyl chains, Bloom[33] has shown that the observed second moment of the ^{1}H lineshape of the alkyl chains in DPPC can be expressed as follows:

$$M'_{2r}(\text{chain}) = M_{2r}(\text{all-}trans) \times S_{dip}^2 \tag{7}$$

where S_{dip} is an average dipolar pseudo-order parameter.

Now, if we examine the spectrum of DMPC shown in fig. 2(*a*), we find from the integrated areas of the $(CH_2)_{10}$ centreband and spinning sidebands, and after taking into account pulse power fall-off, that $M'_{2r}(\text{chain}) = 4.30 \times 10^8\ \text{s}^{-2}$. Insertion of this value into the above equation, and assuming that the second moment of the all-*trans* alkyl chain should be reduced by axial rotation [yielding $M_{2r}(\text{all-}trans) = 4.26 \times 10^9\ \text{s}^{-2}$][35] gives an average molecular order parameter, S_{mol}, of 0.32 for DMPC at 36 °C; if we choose the rigid-lattice value of M_2 of $1.35 \times 10^{10}\ \text{s}^{-2}$ used by Bloom *et al.*, we obtain $S_{dip} = 0.18$. These values are to be compared with an average ^{2}H quadrupole order parameter of 0.18 for [$^2H_{54}$]-DMPC at 36 °C, which yields a molecular order parameter, S_{mol}, of 0.36.[36] Our results can also be compared with the reported order parameter for DPPC (at 50 °C, 9 °C above T_c) of $S_{dip} \approx 0.17$, calculated by Bloom *et al.*[33] Clearly then, there seems to be some promise in using ^{1}H MAS NMR SSB intensities to obtain order-parameter information in membrane systems. In the case of *e.g.* DMPC, close examination of fig. 2(*a*) strongly suggests that MAS experiments at even slower spinning rates should yield order-parameter information for each of the resolved resonances. For example, the terminal methyl and choline methyl peaks have very small first spinning sidebands, which must be due to far smaller order-parameter values (a result not unexpected, based on previous ^{2}H NMR experiments by Gally *et al.*,[37] which did, however, require specific ^{2}H-labelling). Further work should lead to order-parameter values of many resolved sites in a variety of liquid-crystalline phase lipids.

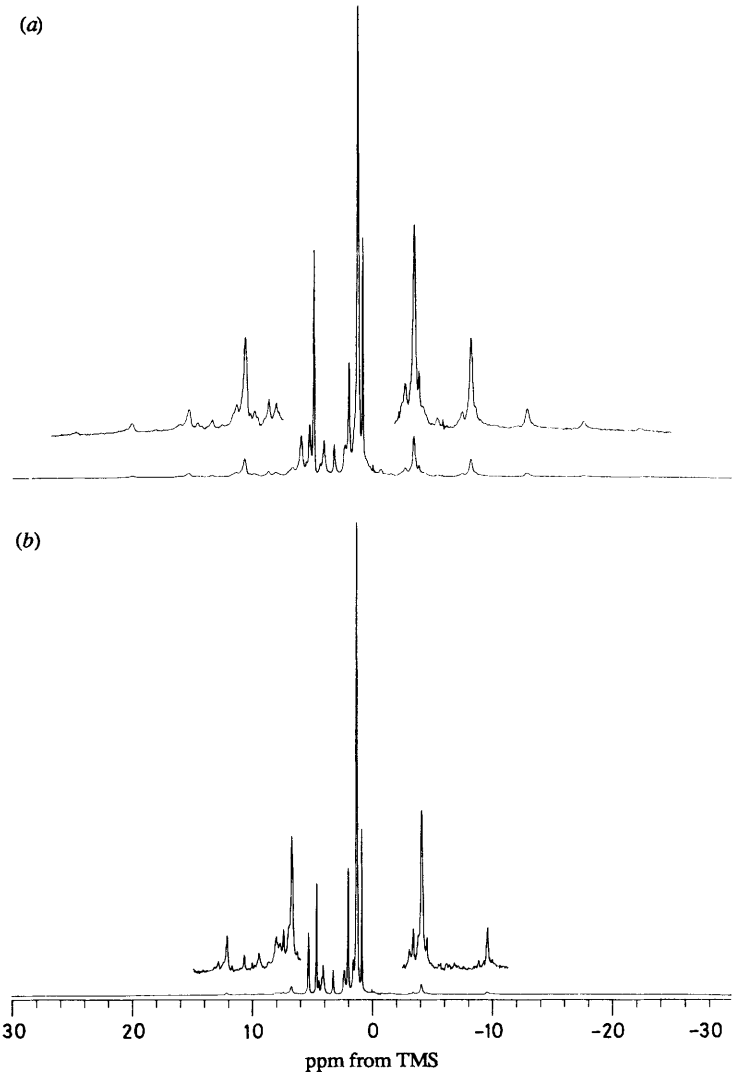

Fig. 3. 500 MHz ^{1}H Fourier-transform MAS NMR spectra of smectic and hexagonal (H_{II}) phase 1,2-dioleoyl-*sn*-glycero-3-phosphoethanolamine–^2H_2O (50% wt). (*a*) 0 °C, smectic phase, 2.4 kHz MAS. (*b*) 30 °C, H_{II} phase, 2.7 kHz MAS. Recycle times of 5 s and an exponential line-broadening of 5 Hz were applied to both spectra.

Other Liquid-crystalline Phases also yield High-resolution Proton Spectra

All of the high-resolution results we have shown above, and most of those reported elsewhere,[19, 20] have been obtained on smectic liquid-crystalline phase lipids. As expected, ^{1}H MAS NMR experiments on the crystalline gel state of lipids yield rather poorly resolved spectra,[20] owing to the increased importance of *inter*molecular dipole–dipole interactions in the gel phase (and perhaps due also in part to the decreased rate of axial rotation). Fortunately, however, other fluid liquid-crystalline phases are also readily amenable to high-resolution ^{1}H MAS NMR, and we show in fig. 3 and 4 typical results on 1,2-dioleoyl-*sn*-glycero-3-phosphoethanolamine (DOPE)–D_2O, and the thermotropic mesogen, MBBA [*N*-(4-methoxybenzylidene)-4′-n-butylaniline].

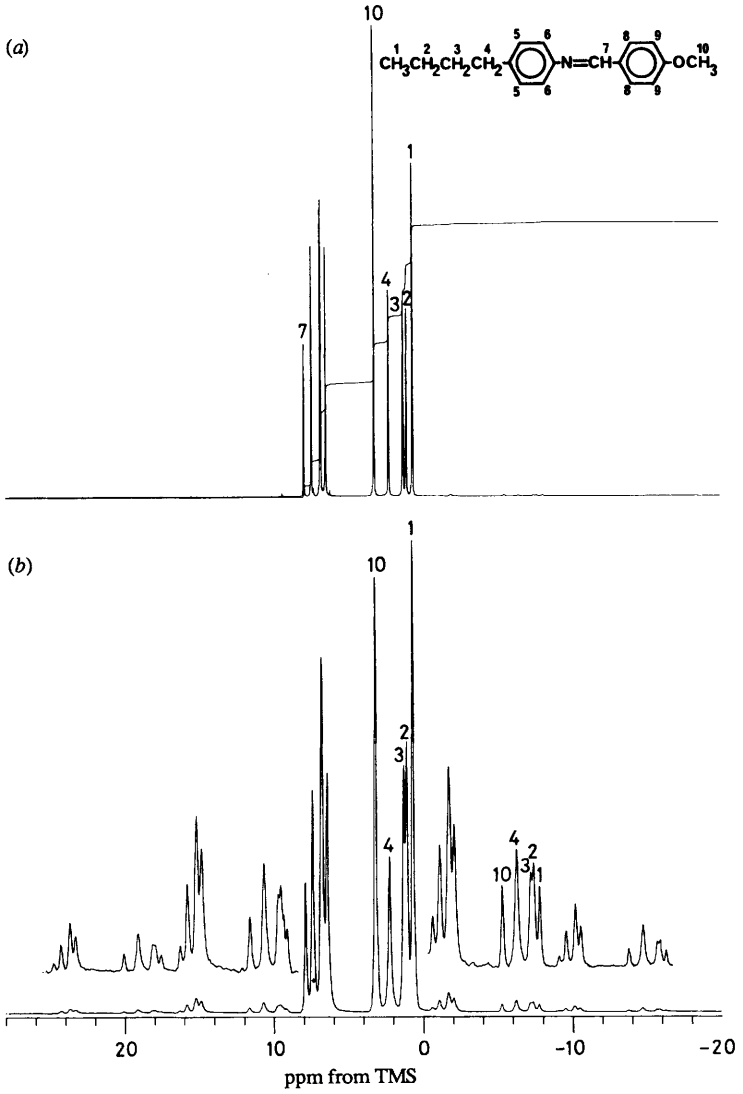

Fig. 4. 500 MHz ^{1}H Fourier-transform MAS NMR spectra of isotropic and nematic phase *N*-(4-methoxybenzylidene)-4′-n-butylaniline (MBBA). (*a*) Isotropic phase, 50 °C, 300 acquisitions. (*b*) Nematic phase, 22 °C. 1000 acquisitions. Tentative assignments are indicated. The MAS rate in both spectra was 4.2 kHz, the recycle times were 5 s and an exponential line-broadening of 5 Hz was utilized.

We show in fig. 3 the 500 MHz ^{1}H MAS NMR spectra of DOPE–50 wt% D_2O at 0 °C [fig. 3(*a*)] and 30 °C [fig. 3(*b*)]. As with the ^{1}H MAS NMR spectra of DMPC at 30 °C (fig. 2), the DOPE spectrum at 0 °C is characteristic of a fluid, smectic liquid-crystalline mesophase, with *ca.* five sets of spinning sidebands being visible. As with DMPC, the centre-band region contains resonances from each of the major lipid groupings present, with decreasing structure being visible in the sidebands. On increasing the temperature from 0 to 30 °C, DOPE (in excess water) passes through a well characterized[38] smectic to hexagonal-II (H_{II}) phase transition. In the H_{II} phase the lipid sheets are arranged in 'tubes', and rotational diffusion occurs around the tube axis.

This has been shown to cause further averaging of the headgroup ^{31}P chemical-shielding anisotropy, by a factor of $-1/2$.[38] Essentially identical results are seen in the ^1H MAS NMR spectrum [fig. 3(*b*)]. Thus the central region of both the smectic and H_{II} phase lipid samples give rise to 'conventional' high-resolution ^1H MAS NMR spectra (fig. 3(*a*) and (*b*)], while the spinning sidebands in the H_{II} phase [fig. 3(*b*)] are markedly reduced from the intensities exhibited in the smectic phase [fig. 3(*a*)], consistent with a reduction in order parameter by a factor of $(-)1/2$, or a reduction in M_{2r} by a factor of 4.

We show in fig. 4 the 500 MHz ^1H MAS NMR spectra of the room-temperature thermotropic nematic mesogen *N*-(4-methoxybenzylidene)-4′-n-butylaniline (MBBA) at 50 °C [isotropic phase, fig. 4(*a*)] and at 22 °C [nematic phase, fig. 4(*b*)]. The results we have obtained on MBBA are basically similar to the 60 MHz MAS NMR results on 4-n-hexyloxyphenyl-4′-methoxybenzoate obtained by Schneider *et al.*,[39] but, just as was the case with our 60 MHz work in 1971–72, low-field operation naturally causes a loss of spectral resolution, and the potentially useful spinning-sideband information was also not reported by Schneider *et al.*[39]

However, since we have not yet made a detailed analysis of the results of fig. 4, and because MAS NMR experiments on nematogens are expected to be quite complex,[40] we simply note here that high-resolution ^1H MAS NMR spectra of nematic-phase liquid crystals, in which all major sites are resolved, can be readily obtained, and moreover, the resultant spinning sidebands in the nematic phase appear to map out the static ^1H spectrum (whose width is *ca.* 30 kHz). The results of fig. 4(*b*) also show that there appears, as with the smectic-phase lipids, to be a considerable amount of information to be gleaned from a full analysis of the SSB intensities. For example, it seems not unreasonable to suppose that the two most intense peaks, at $\delta = 3.16$ and 0.60 ppm, arise from the 4-OMe and 4′-n-butylmethyl groups, based on their total integrated intensity, their chemical-shift values and on the fact that their intensities fall off rapidly with sideband number [fig. 4(*b*)], consistent with a small second moment due to internal C_3 rotation, and perhaps due also to some 'sidechain mobility'. In any case, further ^1H MAS NMR studies seem worthwhile, and we have already obtained two-dimensional NMR on isotropic and nematic MBBA.[41]

Proton MAS NMR Spectra are similar to Sonicated Spectra

We show in fig. 5 representative 500 MHz ^1H NMR spectra of egg-yolk lecithin in an excess of water at 21 °C. Results similar to those in fig. 5(*b*) have appeared previously,[42] but they serve here to illustrate the important point that in ^1H NMR spectroscopy, MAS NMR spectra [fig. 5(*a*)] and spectra of sonically dispersed samples without MAS [fig. 5(*b*)] are similar, at least in the region of the centreband of the spectrum, but they are far from identical. In particular, in the MAS NMR spectrum [fig. 5(*a*)] considerable spectral intensity appears in the spinning sidebands, while in the spectrum of the sonicated material [fig. 5(*b*)] much intensity lies in the (difficult to integrate) broad, non-Lorentzian wings of the spectrum, a feature even more apparent in cholesterol (CHOL)-containing samples (*vide infra*).

Addition of CHOL at 1 : 1 mole ratios (again in an excess of water) causes a broadening of the lipid $(CH_2)_n$ resonance in both MAS and sonicated spectra [fig. 6(*a*) and (*b*)]. As with the pure lipid system, the centreband regions of the MAS and sonicated spectra are quite similar [fig. 6(*a*) and (*b*)], but again there are major differences in lineshape. For example, the $(CH_2)_n$ peak, which is narrow and has SSBs in the MAS NMR spectrum, is broad and non-Lorentzian in the sonicated sample. In addition, in neither spectrum can peaks due to the bulky steroid nucleus be observed, as first reported with sonicated systems by Darke *et al.*[42] and by Kroon *et al.*[43] (with a deuterated lecithin).

As with the case of the pure lipid bilayers (fig. 5), additional spectral intensity in the MAS NMR spectrum arises from numerous sharp, spinning sidebands [fig. 6(*a*)], and

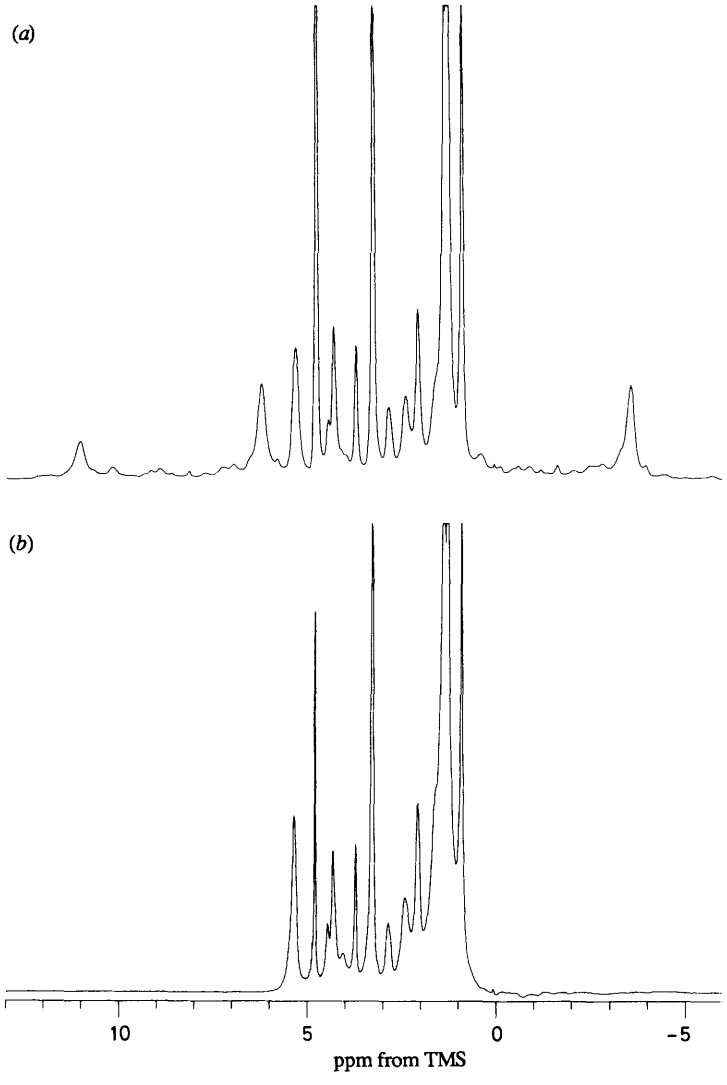

Fig. 5. 500 MHz ^1H Fourier-transform NMR spectra of egg-yolk lecithin (EYL) at *ca.* 21 °C. (*a*) MAS NMR spectrum of a 50 wt % hand dispersion of EYL in ^2H_2O. (*b*) Conventional FT NMR spectrum of a 10 wt % sonicated dispersion of EYL in ^2H_2O. Recycle times of 5 s were used in both cases, as was an exponential line-broadening of 8 Hz.

integrated intensity measurements reveal that essentially all lecithin protons are visualised. The origins of the broad CHOL spectra (in both systems) are not fully understood by us at this time, but appear to arise from short T_2, rather than long T_1, values. Why MAS is unsuccessful in narrowing the CHOL proton spectrum is unclear at present, unless its lateral diffusion or axial rotation is relatively slow, which both seem unlikely. Interestingly, ^{13}C NMR results again do not reveal sharp CHOL features in sonicated vesicles;[19] however, MAS NMR peaks *are* very narrow. Thus, as discussed in detail below, there are very considerable advantages to the use of ^{13}C MAS NMR spectroscopy for the investigation of the rigid CHOL (and other sterol) nucleus, in both model membranes, and in intact biological membranes themselves. ^1H MAS thus

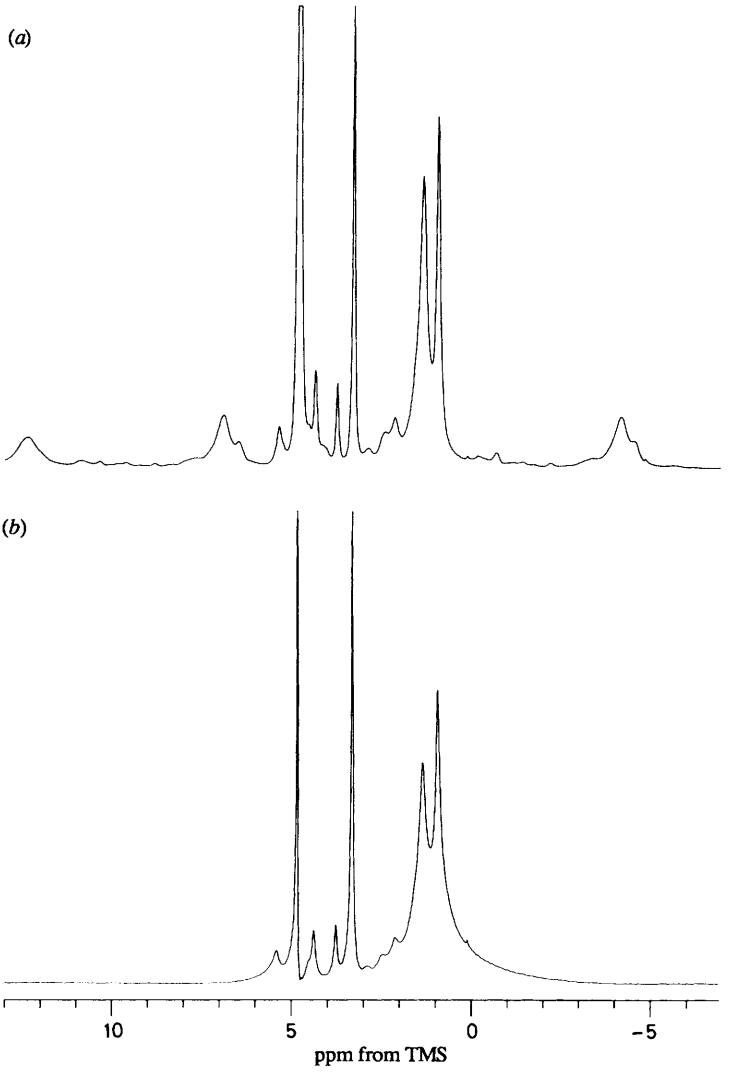

Fig. 6. 500 MHz ^{1}H Fourier-transform NMR spectra of egg-yolk lecithin–CHOL (1:1) at *ca.* 21 °C. (*a*) MAS NMR spectrum of a 50 wt% hand dispersion of EYL–CHOL (1:1) in ^2H_2O. (*b*) Conventional FT NMR spectrum of a 10 wt% sonicated dispersion of EYL–CHOL (1:1) in ^2H_2O. Recycle times of 5 s were used in both cases, as was an exponential line-broadening of 8 Hz. Note the presence of spinning sidebands in the MAS NMR spectrum and a broad, non-Lorentzian lineshape in the sonicated dispersion.

appears primarily useful for investigating the non-steroidal lipids in membranes, while ^{13}C MAS is applicable to both lipids and sterols, although it is, of course, far less sensitive.

Spin-diffusion and Relaxation can be studied *via* Proton MAS

Early work on ^{1}H spin–lattice relaxation in unsonicated lipid bilayers invoked the occurrence of spin diffusion to explain the apparently single T_1 value obtained,[44] a view

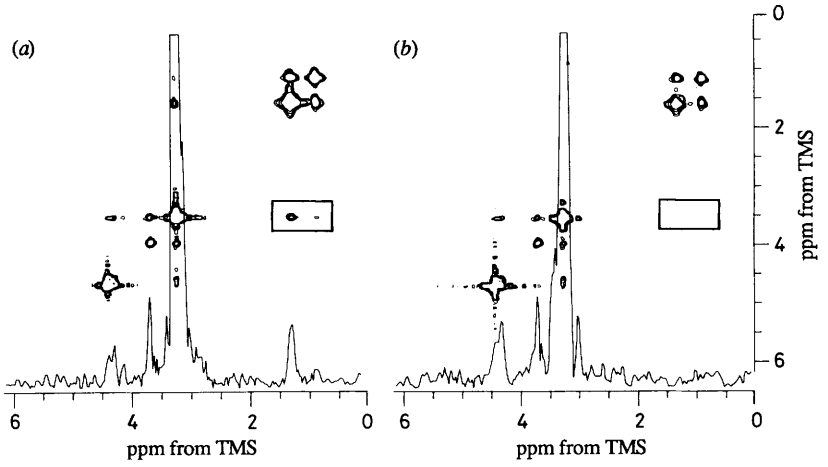

Fig. 7. 500 MHz two-dimensional ^{1}H Fourier-transform NOESY contour plots of unlabelled and ^{2}H-labelled DPPCs at 50 °C, using a 500 ms mix time [see ref. (47) for details of the pulse sequence and phase-cycling used]. (*a*) DPPC (50 wt%) in D_2O, at a spinning speed of 3.3 kHz. (*b*) 1:1, [$^2H_9$]-DPPC:[$^2H_{62}$]-DPPC in D_2O (50 wt%) at a spinning speed of 3.4 kHz. Cross-sections at $\omega_1 = 3.3$ ppm are shown superimposed on the two-dimensional spectra to emphasize the connectivities. 256 files of 1k points, 32 acquisitions per file, at a recycle time of 5 s, were used for data acquisition.

that was challenged later because of the observation of multiple T_1 values, albeit from a sonicated system.[45,46] More recently, this controversial question has arisen again, this time in the context of two-dimensional (2D) NOESY results.[47,48] Thus Xu and Cafiso,[47] studying a sonicated DPPC system in its liquid-crystalline phase, noted cross-peaks between the terminal methyl and choline NMe_3 protons. Based on the results of experiments with a partially deuterated chain-containing DPPC, these workers ruled out spin diffusion, and concluded that chain bends, or chain interdigitation, could cause the terminal methyl groups to be in close spatial proximity to the headgroup protons. Gabriel and Roberts,[48] using a slightly different single unilamellar vesicle system, concluded, however, that spin diffusion could cause such cross-peaks, based on the results of their NOESY experiments on mixed deuterated phospholipids. Thus these workers found cross-peaks in mixed short-/long-chain lecithin vesicles, but no cross-peaks for a mixed system in which the NMe_3 group was deuterated for *ca.* $\frac{1}{2}$ the molecules, while the chains were deuterated in the remaining molecules. If bends/interdigitation were responsible, cross-peaks in the mixed deuterated system would still have been expected (but would have had a smaller intensity).

We have carried out a similar series of experiments on DPPC multi-bilayers, at 51 °C, in an excess of water (fig. 7). In unlabelled DPPC (fig. 7(*a*)] we find weak, but real, cross-peaks between the terminal Me and choline NMe_3, and between the $(CH_2)_{12}$ and the choline NMe_3 resonances, in the 500 MHz 2D NOESY ^{1}H MAS NMR spectra. This could imply chain bends/interdigitation, or spin diffusion, or possibly both. However, in the 2D NOESY spectrum of a 1:1 mixture of [$^2H_{62}$]-DPPC/[N-Me_3-$^2H_9$]-DPPC [fig. 7(*b*)], we find no evidence of any cross-peaks in the corresponding region of the 2D spectrum [shown in the rectangular box in fig. 7(*b*)]. This effect is even more pronounced in cross-sections taken along ω_1 at 3.3 ppm, shown superimposed on the contour maps in fig. 7(*a*) and (*b*). We believe these results indicate that chain bends or interdigitation are thus unlikely to be the origin of the cross-peak intensities observed in fig. 7(*a*), which implies that spin diffusion is responsible for these features. Selective

deuteration of the NMe_3 group in one half of the molecules, and of the acyl chains in the other half, stops intramolecular NMe_3—$(CH_2)_{12}$ spin diffusion, and intermolecular effects are expected to be weak, owing to fast lateral diffusion. If the chains were bent or interdigitated, there should still be weak cross-peaks in the mixed deuterated sample, unless of course there were liquid–liquid immiscibility between the two types of deuterated molecule, which seems rather improbable. We thus believe that spin diffusion, albeit rather weak owing to the reduced spectral overlaps of the chemically shifted peaks, does occur in non-sonicated liquid-crystalline lecithin bilayers under MAS conditions, which implies that it also occurs in non-sonicated samples without MAS.

We have suggested above that such spin diffusion may be rather weak, because we have already observed, in unsonicated bilayers and using ^1H MAS, differential T_1 values between the various chemically shifted groups, as discussed below. Clearly, if spin diffusion were strong, then there would be a single T_1 value characterizing the entire lecithin molecule, in much the same way that one T_1 (or $T_{1\rho}$) value characterizes the spin–lattice relaxation of n-alkanes in the solid state.[49,50]

We thus show in fig. 8 the results of representative T_1 [180°–τ–90°, fig. 8(*a*)], T_2 [90°–τ–180°, fig. 8(*b*)], and $T_{1\rho}$ [90°_x–θ°_y, fig. 8(*c*)] relaxation time measurements on liquid-crystalline DMPC (at 36 °C, in an excess of water), again using 500 MHz ^1H MAS. Also shown in the figure are the T_1, T_2 and $T_{1\rho}$ values obtained. With the exception of the terminal methyl ($T_1 \approx 1.1$ s), all T_1 values in DMPC at 36 °C are in the range 0.5–0.83 s, a surprisingly small range considering the widely different types of motion undergone by the various groups, as judged, for example, from their ^2H NMR order parameters[37] or ^1H SSB intensity profiles (fig. 2).

While it is possible that collective order fluctuations may dominate relaxation, the relaxation rate would then be proportional to S^2, where S is the relevant order parameter. This seems unlikely, given the very small range of relaxation times we observe experimentally. The situation is undoubtedly complex, however, and frequency, temperature and isotopic dilution experiments are currently underway in our laboratory to dissect the various relaxation mechanisms involved.

Carbon-13 MAS yields High-resolution in both Solid and Fluid Phases

This statement should come as no surprise to solid-state NMR spectroscopists, yet surprisingly little work has been reported to date on solid-state ^{13}C NMR of lipids.[19,21–23] In particular, the effects of CHOL on the lipid bilayer have not been reported, neither have the general chemical-shift trends due to phase transitions, or to CHOL incorporation. These topics appear to be a prerequisite to analysis of the more important biological membranes discussed below; thus we will briefly outline our recent results here.

Fig. 9 shows the ^{13}C MAS NMR spectra (proton-decoupled Bloch decays, to ensure reasonable quantitation) of beef-brain galactocerebroside, a natural-occurring primarily C_{24}-hydroxy fatty acid containing cerebroside, having the typical structure:

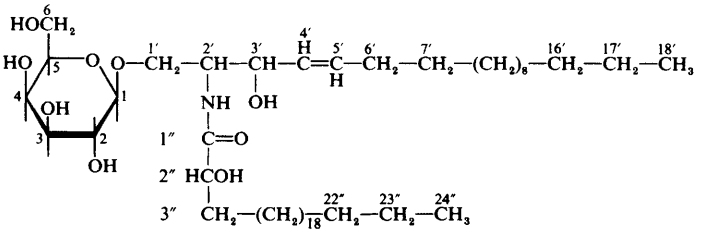

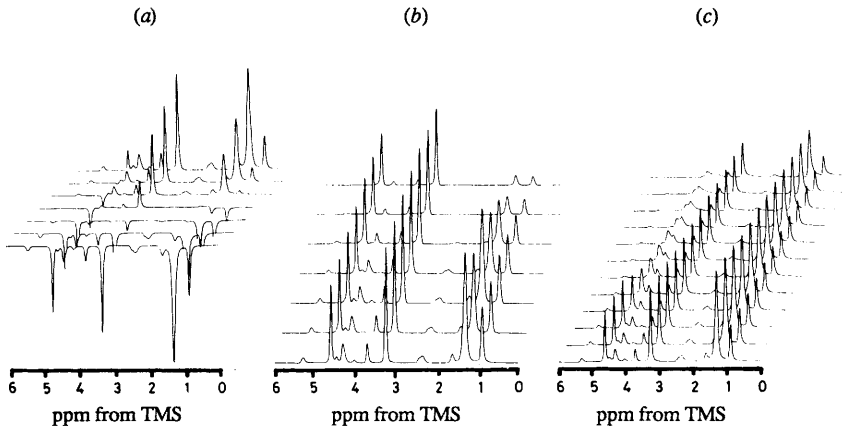

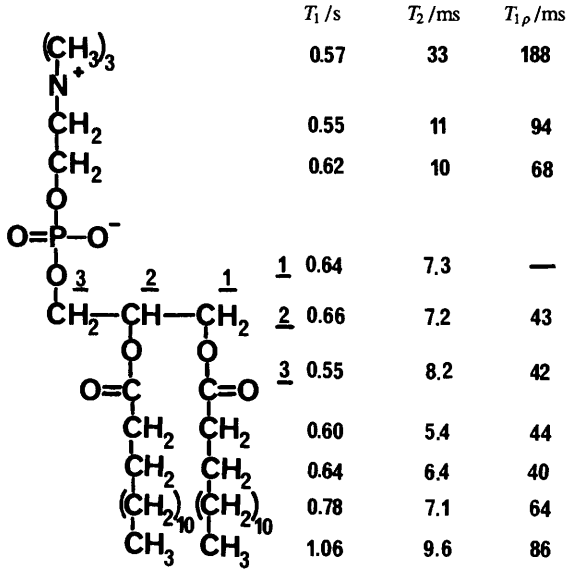

Fig. 8. 500 MHz ^{1}H Fourier-transform MAS NMR determinations of spin–lattice (T_1), spin–spin (T_2) and rotating-frame spin–lattice ($T_{1\rho}$) relaxation times of DMPC–^2H_2O (50 wt%), at 36 °C. (*a*) T_1 (180°–τ–90° sequence) data, (*b*) T_2 (90°–τ–180° sequence) data and (*c*) $T_{1\rho}$ (90°_x–θ°_y sequence, $H_1 \approx 5$ G) data. The relaxation values obtained are shown adjacent to the DMPC structure.

Cerebrosides are sugar lipids, based on a so-called sphingosine back-bone, which has a fatty acid attached to the amino group at C-2′, and a sugar group, in this case galactose, at C-1′. These glycolipids disperse in basically the same way in an excess of water as do phospholipids, forming, at suitable temperatures, smectic liquid-crystalline phase lipid bilayers.[51] In the case of the bovine galactocerebroside studied here, the phase transition from crystalline to liquid-crystalline phase is broad, but is completed by 80 °C.

Fig. 9(*a*) shows the ^{13}C MAS NMR spectrum of bovine galactocerebroside at 21 °C (crystalline state), and in fig. 9(*b*) we show the ^{13}C MAS NMR spectrum of the same

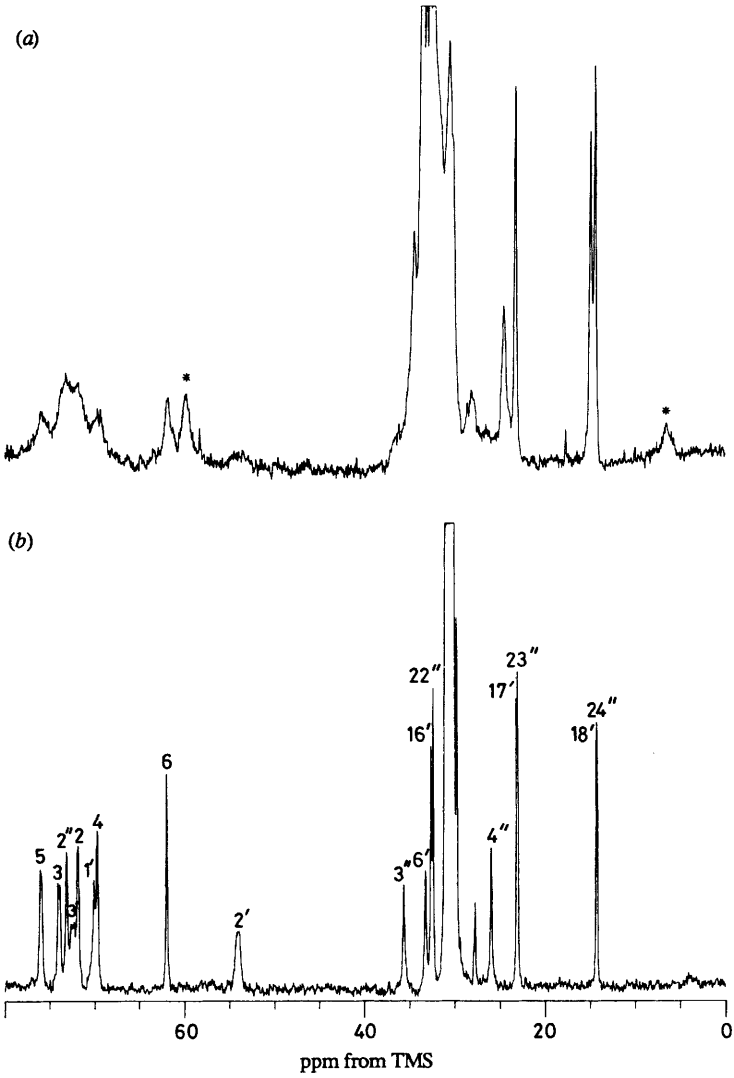

Fig. 9. 125 MHz proton decoupled ^{13}C Fourier-transform MAS NMR spectra of bovine-brain galactocerebrosides (containing primarily C-24 α-hydroxy fatty acids) in an excess of water. (*a*) 21 °C, crystalline phase. (*b*) 80 °C, liquid-crystalline phase. Recycle times of 5 s, 200 acquisitions, 3.3 kHz spinning speed, and an exponential line-broadening of 6 Hz were used in both spectra. Assignments given follow those of Dabrowski *et al.*[59] * indicates a spinning sideband.

sample, but at 80 °C (liquid-crystalline state). There are a number of interesting differences between the two spectra, many of which are not repeated in the ^{13}C results obtained for DPPC (fig. 10) to be discussed below.

The first obvious difference between fig. 9(*a*) and (*b*) is that the resonances in the crystalline cerebroside [fig. 9(*a*)] are in general much broader than the liquid-crystalline phase linewidths [fig. 9(*b*)]. While this might be a general feature of crystal (or gel)–liquid-crystal phase spectral comparisons, it is not, as can be seen by comparison of the gel and liquid-crystalline phase spectra of DPPC shown in fig. 10, and as noted elsewhere by Griffin and coworkers[21] and by de Haan *et al.*[23] We believe that the results of fig. 9(*a*)

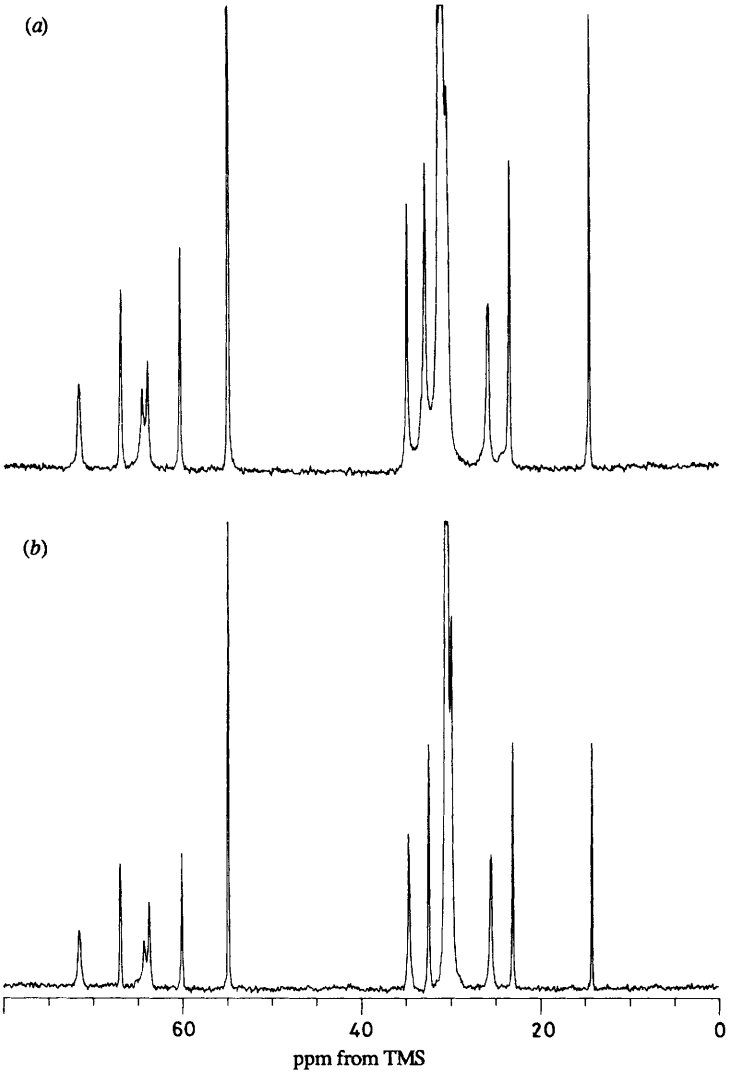

Fig. 10. 125 MHz proton-decoupled ^{13}C Fourier-transform MAS NMR spectra of gel and liquid-crystalline phase DPPC in an excess of water. (*a*) 21 °C, 3.2 kHz MAS, 2500 acquisitions. (*b*) 51 °C, 3.1 kHz MAS, 1096 acquisitions. Recycle times of 5 s, and an exponential line-broadening of 6 Hz were used for both spectra.

are due to the extremely complicated phase behaviour, and hydration characteristics, of cerebrosides, as discussed for example by Ruocco *et al.*[51] More specifically, in the bilayer interior, the acyl chains and sphingosine sidechains are in a reasonably ordered environment and give rise to relatively narrow linewidths, although chain non-equivalences are clearly more pronounced in the crystalline-phase lipid than in the liquid-crystalline state, with respect to both chemical shift and linewidth fig. 9(*a*) and (*b*). Based purely on chemical-shift considerations, we cannot specifically assign the peaks in fig. 9(*a*) at *ca.* 22 ppm to C-17′, C-23″ or *ca.* 14 ppm to C-18′, C-24″ and specific ^{2}H-labelling of *e.g.* the C-24 fatty acid will be necessary to make assignments, which may,

however, yield interesting information on chain packing for such mixed long/short-chain lipids.

Another major difference between the two spectra in fig. 9 is that the isotropic chemical shift of the largest peak in the spectrum, arising from the bulk of the chain CH_2 groups, is deshielded by *ca.* 2.3 ppm in the crystalline *vs.* liquid-crystalline state. We believe this effect originates in the increased population of all-*trans* hydrocarbon chain configurations in the crystalline state, or conversely, that the presence of *gauche* containing bends or kinks in the liquid-crystalline phase causes an increased shielding. If this idea is correct, it could obviously lead to a determination of the percentage of *gauche* isomers, and to effective chain lengths, in much the same way that ^2H NMR has been used in the past.[52] An attractive possibility would be to use such an approach to study biomembranes themselves.

The third major difference between the crystalline and liquid-crystalline phase results shown in fig. 9 is that there is clearly a major line-broadening in the sugar/backbone region in the crystalline-phase spectrum fig. 9(*a*). For example, the resonance at *ca.* 62 ppm in both spectra, due to C-6 of the galactose residue (CH_2OH), has a linewidth of *ca.* 80 Hz in the crystalline phase, but only 14 Hz in the liquid-crystalline phase. These differences are not due to inadequate proton decoupling, so they must represent either intermediate exchange between conformational isomers, or perhaps more likely, they could be due to a distribution of isotropic chemical shifts caused by a range of conformations, and/or of degrees of hydration of the headgroup region, a notion not inconsistent with the slow hydration of cerebroside bilayers noted previously using scanning calorimetry.[51] Interestingly, broad ^{13}C spectra of amorphous sugars are well known,[53] and we may be seeing a reflection of a not dissimilar random packing in the headgroup region of this crystalline sugar lipid. More detailed studies of cerebrosides are currently underway.

We show in fig. 10 the 125 MHz ^{13}C MAS NMR spectra of DPPC, hand-dispersed in an excess of water (D_2O) at 21 °C (*a*) and 51 °C (*b*). The gel-to-liquid-crystalline phase transition temperature of DPPC is 41 °C.[54] Clearly, there are much greater similarities between the results of fig. 10 than were obtained between the results of fig. 9, and indeed there is no marked difference between the two data sets. However, close examination of the isotropic chemical shifts reveals (table 1) that there are definite deshieldings in these shifts upon lowering temperature, which amount to *ca.* 0.6 ppm for C5-13, 0.5 ppm for C-4, and *ca.* 0.3–0.4 ppm for C-14 to C-16. We believe these results reflect the fact that the gel state of lecithin is quite disordered (fast axial rotation plus significant *gauche–trans* isomerization), consistent with the early wide-line work of Veksli *et al.*[2]

Now, upon addition of CHOL (at 1:1 mole ratios, in an excess of D_2O), we obtain the results shown in fig. 11(*a*) and (*b*). Again, there are large similarities between the results obtained at 21 °C [fig. 11(*a*)] and 51 °C [fig. 11(*b*)], as shown in table 2. The first obvious difference between these results and those of pure DPPC (fig. 10) is that a large number of additional peaks, due to CHOL, have appeared. Note that in the ^1H MAS NMR results shown in fig. 6 we did not observe much in the way of intensity from CHOL, presumably owing to T_2 relaxation. However, in the ^{13}C MAS NMR results, essentially each carbon atom site can be identified, and assigned, although as discussed below, even better resolution of the CHOL peaks can be obtained *via* the use of deuterated lipids and CP, rather than Bloch decay methods. Also, the observation of CHOL peaks in the DPPC–CHOL system *via* MAS is to be contrasted with the almost total inability to obtain any useful information about the CHOL nucleus in conventional ^{13}C FT NMR spectra of sonicated dispersions,[24] at least at high CHOL levels.

The major difference which can be seen from comparison of the results of fig. 11(*a*) and (*b*) is that the large peak centred at *ca.* 31 ppm in the 51 °C spectrum [fig. 11(*b*)] is deshielded by *ca.* 1 ppm upon cooling the sample to 21 °C [fig. 11(*a*)]. Similar *ca.* 1 ppm deshielding effects can be attributed to the mere addition of CHOL, at either 21 or

Table 1. Chemical-shift assignments for DPPC in gel (21 °C) and liquid-crystalline (51 °C) phases compared with solution assignments

assignment	δ (ppm) from TMS		
	21 °C	51 °C	solution[a]
chain-C1 (C=O)	174.1[b]	173.9[b]	174.7 174.3
glycerol-C2	71.5	71.5	72.5
choline-Cβ	66.8	66.9	67.7
glycerol-C3	64.5	64.3	64.9
glycerol-C1	63.8	63.7	64.4
choline-Cα	60.2	60.0	60.8
choline-Cγ	54.9	54.9	55.7
chain-C2	34.8	34.7	35.9
chain-C14	32.8	32.4	33.4
chain-(C5–13)	31.1	30.5	31.2
chain-C4	30.4	29.9	[c]
chain-C3	25.8 25.7	25.5 25.4	26.4
chain-C15	23.4	23.0	24.2
chain-C16	14.5	14.2	15.5

[a] Ref. (34). Shifts given for DPPC in chloroform. [b] Only one carbonyl resonance seen in DPPC–D_2O mixture. [c] Peak could not be resolved at the field used.

51 °C. We believe these results are consistent with our previous observations on cerebroside and on pure DPPC. In each case systems expected to have a more ordered, all-*trans* chain conformation (or at least, to contain less mobile *gauche* conformers) are deshielded in the range *ca.* 0.6 to 1.2 ppm. With further work, we hope to be able to use such isotropic chemical shift information to more quantitatively assess *gauche* chain contents.

Chain Deuteration allows Observation of Most Sterol Sites

Most of the carbons in the CHOL molecule can be observed, and assigned, in the spectra shown in fig. 11, by simple comparison with existing solution spectra of CHOL.[55] However, it would clearly be desirable to eliminate as many of the lipid peaks as possible, to prevent confusing spectral overlaps. We show in fig. 12 that this can be readily accomplished by using a specifically (chain) deuterated lipid, together with cross-polarization techniques.[56] Fig. 12(*a*) shows the CP MAS NMR spectrum of a 1:1 DMPC–CHOL dispersion at 21 °C, in an excess of water, in which both lipid and CHOL peaks can be seen. Deuteration of the acyl chains inhibits the ^{13}C–^{1}H cross-polarization process, and the result, for a [$^{2}H_{54}$]-DMPC–CHOL (1:1) dispersion, is shown in fig. 12(*b*). Essentially all of the intensity arising from the lipid acyl chains is removed, *e.g.* the terminal methyl peak at *ca.* 15 ppm is no longer visible, and more importantly, areas of the spectrum suffering severe spectral overlap, *e.g.* the 30–34 ppm region, are now quite well resolved. In particular, it is not a simple matter to observe and assign the CHOL peaks arising from C-2, C-7 and C-8 at *ca.* 32 and 33 ppm, and such new assignments are included in table 2. The peak at *ca.* 35 ppm, labelled L, is due to residual ^{1}H at C2 of the lipid acyl chain.

Of course, headgroup lipid carbons in the 55–72 ppm region are still visible, since they were not deuterated, but the long T_{CH} values cause them to be severely attenuated in the

Table 2. Comparison of DPPC–CHOL chemical shifts at 21 and 51 °C with solution values

		δ (ppm) from TMS		
		DPPC–CHOL (1:1)		
peak no.[a]	assignment	21 °C	51 °C	solution[b]
1	chain-C1 (C=O)	174.3	174.2	174.7
2		173.9	174.1	174.3
3	chol-C5	142.6	142.6	141.5
4	chol-C6	120.8	121.0	121.6
5	glycerol-C2 chol-C3	71.4	71.6	72.5 71.6
6	choline-Cβ	66.8	67.2	67.7
7	glycerol-C3	64.5	64.5	64.9
8	glycerol-C1	63.9	64.0	64.4
9	choline-Cα	60.2	60.2	60.8
10	chol-C14, C17[c]	57.8	57.8	57.2
		57.6	57.7	56.8
11	choline-Cγ	54.8	55.1	55.7
12	chol-C9	51.0	51.2	50.8
13	chol-C13[d]	43.2	43.4	42.7
14	chol-C4	42.3	42.5	42.7
15	chol-C12	41.0	41.1	40.4
16	chol-C24	40.2	40.2	39.9
17	chol-C1	38.4	38.5	37.8
18	chol-C22, C20	37.5	37.2	36.7, 36.1
19	chol-C10[d]	37.3	37.4	36.8
20	chain-C2	35.0	35.0	35.9
21	chol-C7, C8[e]; chain-C14	32.9	32.7	32.3; 33.4[f]
22	chain-(C5–C13)	32.2	31.4	31.2
23	chol-C2[e]	31.5	[g]	31.9
24	chain C-4	30.8	30.4	[h]
25	chol-C16	29.2	29.1	28.6
26	chol-C25	28.7	28.5	28.3
27	chain-C3	26.1	25.9	26.4
28	chol-C15, C23	25.4	25.6	24.6, 24.4
29	chain-C15	23.4	23.2	24.2
30	chol-C26, C27	23.0	22.9	23.1, 22.8
31	chol-C11	22.1	22.1	21.5
32	chol-C19	20.4	20.2	19.7
33	chol-C21	19.9	19.9	19.1
34	chain C-16	14.4	14.2	15.5
35	chol-C18	13.2	13.1	12.3

[a] Fig. 11. [b] Ref. (34) for DPPC and ref. (55) for cholesterol. Shifts given for DPPC are for the lipid dissolved in chloroform. Shifts given for cholesterol are for the sterol dissolved in dioxane–chloroform. [c] Peaks cannot be assigned on a one to one basis. [d] The quaternary carbons are narrower than protonated sites, so they may be distinguished from the nearby protonated carbons. [e] Peak assigned by comparing to fig. 13(*b*). [f] See table 1 for chain-C14 chemical shifts in DPPC–D_2O. [g] Resonance obscured. [h] Could not be resolved at the field used.

CP experiment, and the resulting spectrum [fig. 12(*b*)], is overwhelmingly dominated by the CHOL resonances.

This approach is naturally not restricted to CHOL, and we show in fig. 13 similar spectra of 25 mol% stigmasterol, desmosterol and lanosterol, all in [$^2H_{54}$]-DMPC at

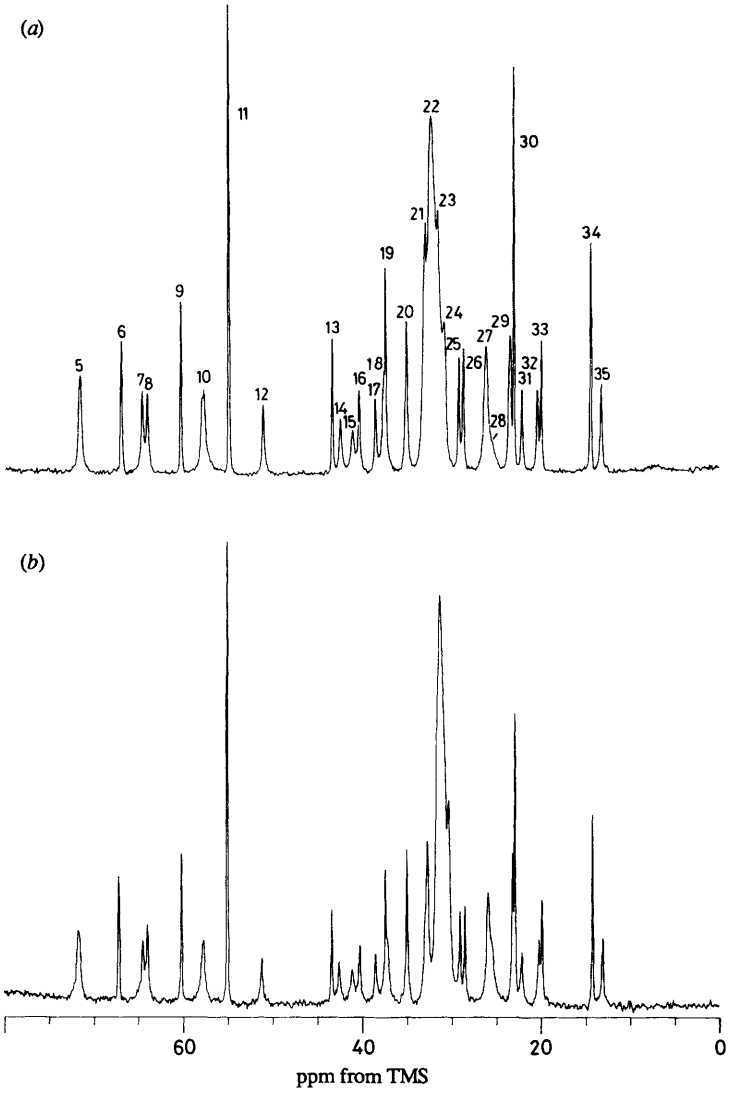

Fig. 11. 125 MHz proton-decoupled ^{13}C Fourier-transform MAS NMR spectra of DPPC–CHOL (1:1) in an excess of water, at 21 and 51 °C. (*a*) 21 °C, 3.0 kHz MAS, 2000 acquisitions. (*b*) 51 °C, 3.3 kHz MAS, 2000 acquisitions. Recycle times of 5 s and an exponential line-broadening of 6 Hz were used for both sets of spectra.

21 °C, in an excess of water. Many spectral assignments can be made, by comparison with solution ^{13}C NMR results, as indicated in fig. 13 and in table 3.

We believe that this approach not only is of utility for simplifying ^{13}C MAS NMR spectra of model lipid–water dispersions, but also should be of help in simplifying spectra of intact biological membranes containing sterols and work on ^{2}H-labelled *Acholeplasma laidlawii* B (PG9) is currently underway. If successful, the results should allow the unambiguous study of CHOL dynamics in an intact biological membrane, including, perhaps, deducing the effects of membrane proteins on CHOL mobility.

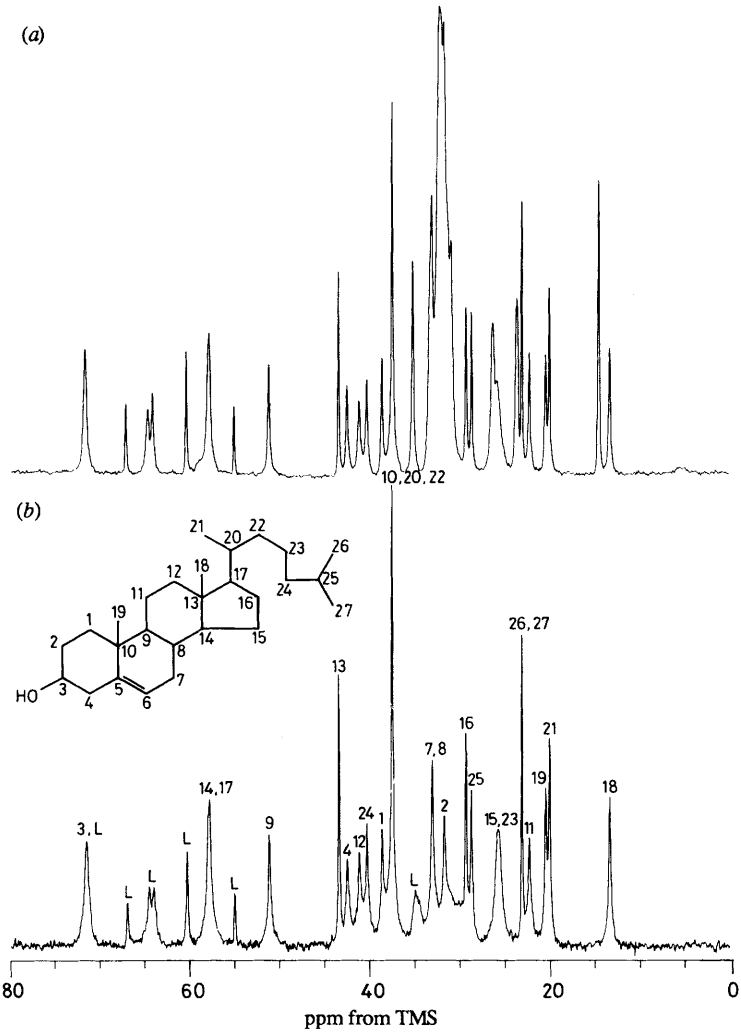

Fig. 12. 125 MHz proton-decoupled cross-polarization ^{13}C Fourier-transform MAS NMR spectra of DMPC-CHOL (1:1) obtained using unlabelled or chain ^{2}H-labelled DMPC at 21 °C and a 5 ms mix time. (*a*) Unlabelled DPPC–CHOL. (*b*) [$^{2}H_{62}$]-DPPC–CHOL. The MAS rate was 3.3 kHz in both cases. Recycle time of 5 s, 2000 acquisitions and an exponential line-broadening of 6 Hz were utilized in both spectra. The cholesterol assignments given are based on literature values for CHOL in $CDCl_3$.[55] Peaks labelled L are lipid resonances.

Difference Spectroscopy permits Study of Hydrocarbon Chains in Membranes

The results of an experiment related to that outlined in fig. 12 are given in fig. 14. Here we show [fig. 14(*a*)] the ^{13}C CP-MAS NMR spectrum of DMPC (at 23 °C, in an excess of water), together with, in fig. 14(*b*), the corresponding spectrum of DMPC, but in the presence of a 1:1 mole ratio of CHOL. CHOL peaks themselves are not visible (or are very weak), since the result shown in fig. 14(*b*) was obtained by taking the difference spectrum between a protonated DMPC–CHOL (1:1) spectrum, and a [$^{2}H_{54}$]-DMPC–CHOL (1:1) spectrum, both in an excess of water at 23 °C. The result of taking

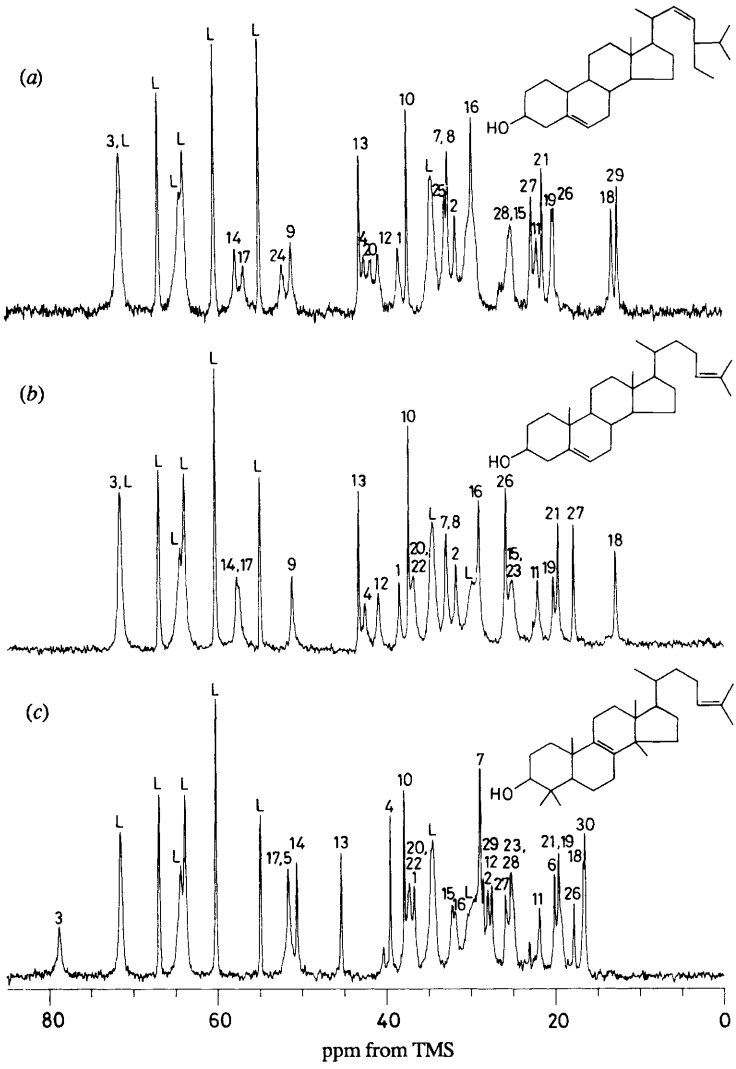

Fig. 13. 125 MHz proton-decoupled ^{13}C cross polarization Fourier-transform MAS NMR spectra of various sterol–[$^2H_{54}$]-DMPC (1 : 3 mole ratio) mixtures in an excess of water at 21 °C, with a 5 ms mix time and a MAS rate of 3.3 kHz. (*a*) Stigmasterol, (*b*) desmosterol and (*c*) lanosterol. Recycle times of 5 s, mix times of 5 ms, 2000 acquisitions and an exponential line-broadening of 6 Hz were applied to each spectrum. Assignments follow those given in the literature.[60–62] Peaks labelled L are lipid resonances.

such a difference spectrum is that essentially all of the CHOL peaks are eliminated, and since the deuterated segments do not cross-polarize, and the unlabelled lipid segments are eliminated by the spectral subtraction, the result is that a lipid hydrocarbon chain spectrum, but reflecting the chemical shifts caused by the addition of CHOL, is obtained [fig. 14(*b*)]. As can be seen in fig. 14(*b*), there are a number of downfield shifts (the shifts are indicated on the figure), which we believe correlate with the increase in *trans* conformers upon addition of CHOL.

Overall, the results of this section and the previous section therefore indicate that

Table 3. Tentative assignments for stigmasterol, desmosterol and lanosterol in [$^2H_{54}$]-DMPC (1:3) based on solution assignments

carbon assignment	δ (ppm) from TMS					
	stigmasterol		desmosterol		lanosterol	
	DMPC–D_2O	solution[a]	DMPC–D_2O	solution[b]	DMPC–D_2O	solution[c]
1	38.3	37.4	38.3	37.3	36.7	35.7
2	31.6	31.7	31.6	31.6	27.9	27.9
3	71.4	71.8	71.5	71.6	78.7	79.0
4	42.4	42.4	42.4	42.3	39.5	39.0
5	142.6	140.9	142.6	140.7	51.6	50.5
6	120.9	121.7	121.0	121.4	20.0	19.2
7	32.5	31.9	32.8	31.9	28.8	28.3
8					135.8	134.4
9	51.0	50.3	51.1	50.2	134.7	134.4
10	37.3	36.6	37.3	36.5	37.9	37.1
11	21.9	21.1	21.9	21.1	21.8	21.1
12	40.7	39.8	40.8	39.8	27.5	26.6
13	43.0	42.4	43.2	42.3	45.3	44.6
14	57.7	57.0	57.6	56.8	50.6	49.4
15	25.0	24.4	25.0	24.8	32.1	31.1
16	29.6	28.9	28.9	28.2	31.8	30.9
17	56.7	56.0	57.4	56.1	51.6	50.7
18	13.1	12.2	12.7	11.9	16.6	15.8
19	20.1	19.4	20.1	19.4	19.5	18.3
20	41.6	40.5	36.7	35.5	37.2	36.6
21	21.3	21.1	19.5	18.6	19.5	18.8
22	139.0	138.4	36.7	36.1	37.2	36.3
23	130.3	129.4	25.0	24.7	25.1	25.0
24	52.1	51.3	125.6	125.0	125.7	125.3
25	32.8	31.9	130.5	130.6	130.4	130.8
26	19.9	19.0	25.7	25.6	17.7	17.6
27	22.5	21.1	17.7	17.6	25.8	25.7
28	25.0	25.4			25.1	24.3
29	12.4	12.0			28.5	28.1
30					16.4	15.4

[a] Ref. (60). [b] Ref. (61). [c] Ref. (62). $CDCl_3$ was used as the solvent for each sterol.

high-resolution solid-state ^{13}C NMR spectra of sterols in membranes, and of lipid hydrocarbon chains in the presence of sterols, can be obtained, by suitable use of deuterated lipids, cross-polarization and difference spectroscopy techniques.

Over Fifty Resonances can be seen in Spectra of some Biological Membranes

The goal of all of the aforementioned techniques is to be able to investigate numerous, resolved, single-carbon atom resonances in intact biological membranes. We show in fig. 15 the first realization of this goal. Fig. 15(*a*) represents the upfield region of the ^{13}C MAS NMR spectrum of human myelin, and in fig. 15(*b*) we show for comparison the ^{13}C MAS NMR spectrum of goldfish myelin (actual species and variety of the latter are rather uncertain). These are by far the highest-resolution spectra ever obtained of a biological membrane. Previous workers have reported related ^1H spectra of sonicated

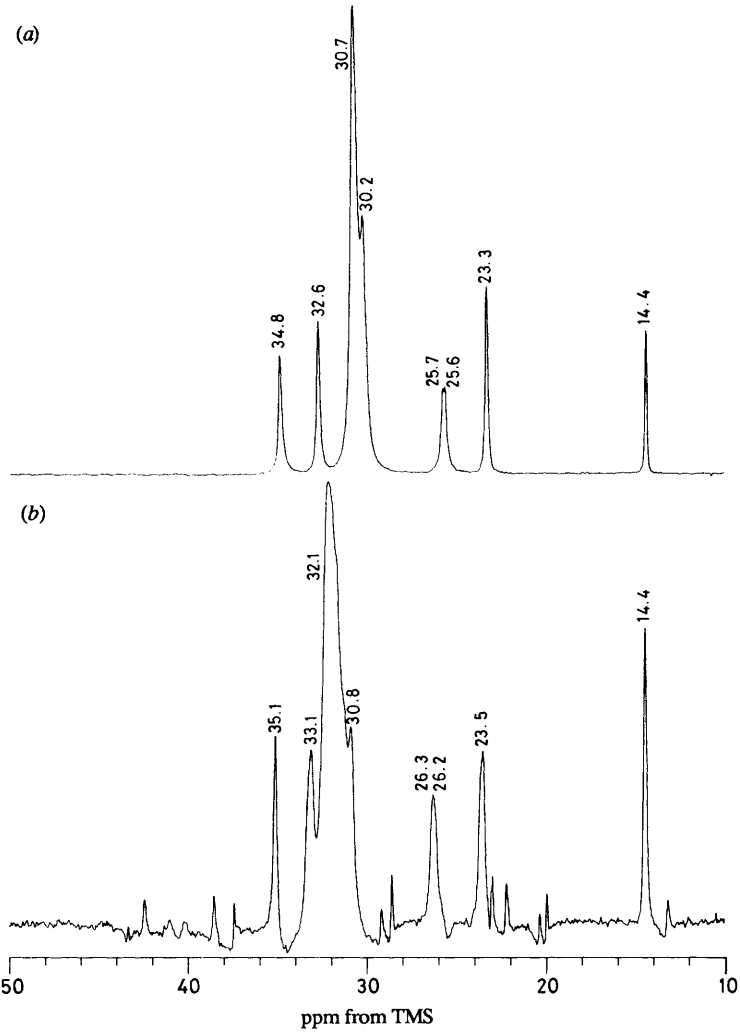

Fig. 14. Comparison of the 125 MHz proton-decoupled ^{13}C Fourier-transform CP MAS NMR spectra of the acyl-chain region of DMPC in the absence and presence of cholesterol. (*a*) ^{13}C CP MAS NMR spectrum of 50 wt% DMPC–D_2O, 10 ms mix time. (*b*) Difference spectrum: [DMPC–cholesterol] – [$^2H_{54}$-DMPC–cholesterol]. The small features represent CHOL peaks which are incompletely suppressed. Note the large deshielding of the chain CH_2 groups upon addition of CHOL. Spectral conditions were basically as outlined in fig. 13.

myelin[5] and ^{13}C spectra of unsonicated myelin,[57] but few well resolved peaks were observed.

Not only can numerous single-carbon atom sites be resolved in the spectra shown in fig. 15, but many of them can be readily assigned by reference to the previous results on lecithin, lecithin–CHOL and cerebroside (the major constituents of myelin are lecithin/sphingomyelin, phosphatidylethanolamine, cerebrosides and cholesterol),[58] as shown in table 4. Interestingly, no features attributable to the *ca.* 20 wt% of membrane protein can be observed, a result consistent with the general lack of ability to observe proteins in membranes without specific enrichment, owing to their rigid nature (large chemical-shift anisotropy), and wide range of isotropic chemical shifts.

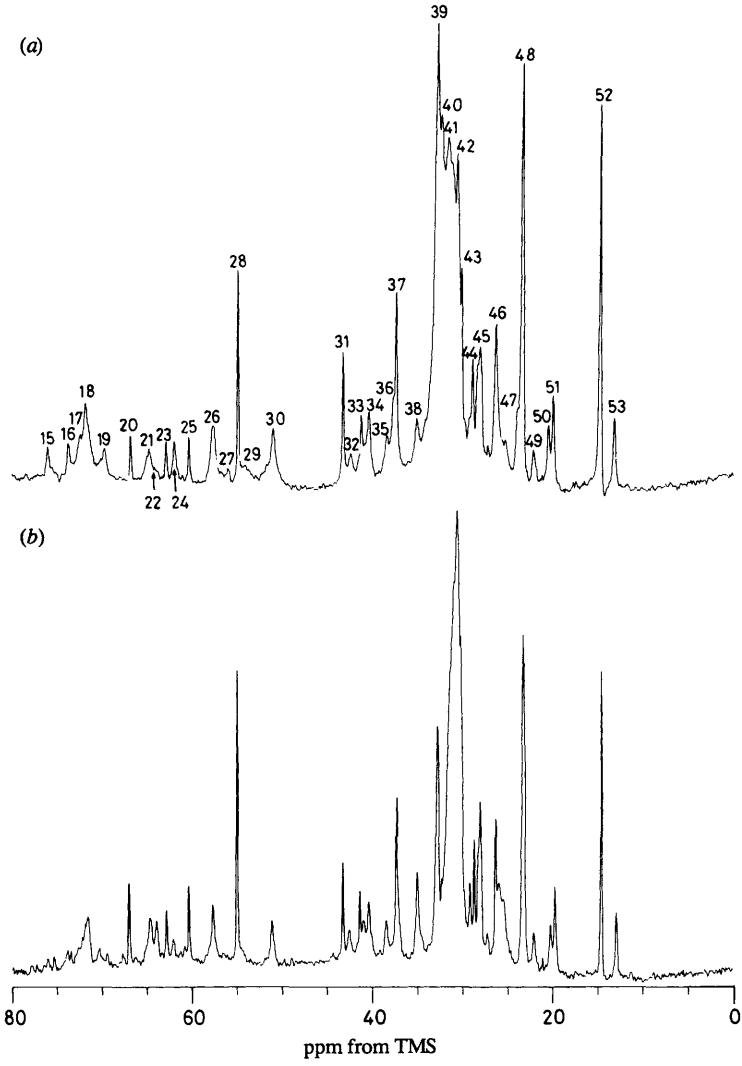

Fig. 15. 125 MHz proton-decoupled carbon-13 Fourier-transform MAS NMR spectra of adult human and goldfish myelins in an excess of water at 21 °C. (*a*) Adult human, 8000 acquisitions. (*b*) Goldfish, 15000 acquisitions. In each spectrum the MAS rate was 3.3 kHz, the recycle time was 5 s and an exponential line-broadening of 6 Hz was applied. Assignments are given in table 4.

The results of fig. 15 are also of interest, since they appear to reflect the ordering effect of CHOL on the lipid hydrocarbon chains in the 30–34 ppm region. Since both spectra were recorded at *ca.* 23 °C, the human myelin is some 14 °C below its 'growth temperature', while the goldfish myelin is some 14 °C above its 'growth temperature'. Our results indicate that the human myelin is thus relatively more ordered with respect to the goldfish myelin, a result confirmed by recent variable-temperature ^{13}C MAS NMR experiments on human myelin (data not shown).

We believe that the ability to obtain highly resolved ^{13}C MAS NMR spectra of intact biological membranes, and to assign many of the peaks to individual atomic sites, offers great promise for future detailed studies of biomembrane structure, including detailed

Table 4. Preliminary myelin carbon-13 resonance assignments

peak no.	myelin δ (ppm)	assignment	model δ (ppm)	peak no.	myelin δ (ppm)	assignment	model δ (ppm)
1	175.5	cerebroside-C1″	176.6[b]	29	54.0	cerebroside-C2′	54.0[b]
		sphingomyelin (C=O)	175.4	30	50.9	chol-C9	51.0[c]
2	174.2	acyl-C1 (C=O)	174.3[c]	31	43.2	chol-C13	43.2[c]
6	134.6	cerebroside-C4′	134.9[b]	32	42.4	chol-C4	42.3[c]
7	130.5	[18:2]-C9[d]	130.5[e]	33	41.6	chol-C12[h]	41.0[c]
8	130.0	[18:1]-C9, C10[d]	130.0[e]	34	40.3	chol-C24	40.2[c]
		cerebroside-C5′	130.1[b]	35	38.3	chol-C1	38.4[c]
9	128.9	[20:4]-C8, C9[d]	128.9[e]	36	37.6	chol-C20, C22	37.5[c]
10	128.6	[18:2]-C10[d]	128.6[e]	37	37.3	chol-C10	37.3[c]
11	128.3	[18:2]-)C12[d]	128.4[e]	38	35.0	acyl-C2	35.0[c]
12	121.4	chol-C6	121.8[c]	39	32.6	chol-C7, C8; C(ω-2); $CH_2)_n^i$	32.9[c]
14	104.0	sugar-C1	104.1[b]	40	32.2	$(CH_2)_n^i$	32.2[c]
15	75.9	sugar-C5	75.9[b,g]	41	31.5	$(CH_2)_n^i$	
16	73.6	sugar-C3	73.9[b,g]	42	30.4	$(CH_2)_n^i$	
17	72.3	cerebroside-C3′, C2″	72.4[b,g], 73.1[b]	43	30.0	$(CH_2)_n^i$	
18	71.7	glycerol-C2, chol-C3	71.4[c]	44	28.8	chol-C25	28.7[c]
		sugar-C2	71.8[b]	45	27.9	[18:1]-C8, C11,[d] [18:2]-C8,C14[d]	28.0[e]
19	69.6	sugar-C4	69.7[b]	46	26.2	acyl-C3, [18:2]-C11[d]	26.1[e]
20	66.7	choline-Cβ	66.8[c]	48	23.3	acyl-C(ω-1)	23.4[c]
21	64.7	PE glycerol-C3	64.5[f]		23.2	chol-C26, C27	23.0[c]
22	64.1	PC glycerol-C1, C3	64.2[c,g]	49	22.1	chol-C11	22.1[c]
23	62.8	ethanolamine-Cα	62.7[f]	50	20.4	chol-C19	20.4[c]
24	61.9	sugar-C6	61.9[b]	51	19.8	chol-C21	19.9[c]
25	60.3	choline-Cα	60.2[c]	52	14.6	acyl-C(ω)	14.4[c]
26	57.5	chol-C14, C17	57.7[c,g]	53	13.1	chol-C18	13.2[c]
28	54.8	choline-Cγ	54.8[c]				

[a] Fig. 15(*a*). [b] Shifts given for liquid-crystalline bovine galactocerebroside at 80 °C, comprised mainly of hydroxy fatty acids; assignments from ref. (59). [c] Shifts given for DPPC–CHOL at 21 °C, see table 2 and ref. (34) and (55). [d] Acyl-chain type given as the most likely type, longer chains with the same amount of unsaturation could give the same shift. [e] Shifts given for egg-yolk lecithin–cholesterol (1:1), ref. (19), the assignments follow ref. (63) and (64). [f] Shifts given for 1,2-dioleoyl-*sn*-glycero-3-phosphoethanolamine multilayers (unpublished results), assignments from ref. (65). [g] Chemical-shift value reported as average of model values, since two resonances were seen. [h] The ethanolamine-Cβ resonance is between peaks 33 and 34 at 40.8 ppm. [i] Cannot be specifically assigned due to spectral overlap.

analysis of the rates and types of motion of each of the major lipid classes, on collective order fluctuations, on the evolutionary development of myelin membranes, on the topic of myelin development and, perhaps, on the changes in membrane structure that occur in various membrane abnormalities.

This work was supported in part by NSF grant DMB 84-16771, NIH grant GM-40426 and by American Heart Association grant 87-0756.

References

1 D. Chapman, R. E. Richards and R. W. Yorke, *J. Chem. Soc.*, 1960, 436.
2 Z. Veksli, N. J. Salsbury and D. Chapman, *Biochim. Biophys. Acta*, 1969, **183**, 434.
3 D. Chapman and S. A. Penkett, *Nature (London)*, 1966, **211**, 1304.
4 D. Chapman, V. B. Kamat, J. De Gier and S. A. Penkett, *J. Mol. Biol.*, 1968, **31**, 101.
5 D. Chapman and V. B. Kamat, *Regul. Funct. Biol. Membranes, Proc. 2nd Sigrid Jusélius Symp.*, ed. J. Järnefelt (Elsevier, Amsterdam, 1968), vol. 11, pp. 99–106.
6 S. Rottem and S. Razin, *J. Bacteriol.*, 1966, **92**, 714; H. O. Hauser, *Biochem. Biophys. Res. Commun.*, 1971, **45**, 1049.
7 O. Bakouche, D. Gerlier, J-M. Letoffe and P. Claudy, *Biophys. J.*, 1986, **50**, 1.
8 M. P. N. Gent and J. H. Prestegard, *Biochemistry*, 1974, **13**, 4027.
9 C. H. A. Seiter and S. I. Chan, *J. Am. Chem. Soc.*, 1973, **95**, 7541.
10 G. J. T. Tiddy, *Nature (Phys. Sci.)*, 1971, **230**, 136.
11 S. I. Chan, G. W. Feigenson and C. H. A. Seiter, *Nature (London)*, 1971, **231**, 110.
12 E. Oldfield, J. Marsden and D. Chapman, *Chem. Phys. Lipids*, 1971, **7**, 1.
13 D. Chapman, E. Oldfield, D. Doskočilová and B. Schneider, *FEBS Lett.*, 1972, **25**, 261.
14 E. Oldfield and D. Chapman, *Biochem. Biophys. Res. Commun.*, 1971, **43**, 949.
15 K.M. Keough, E. Oldfield, D. Chapman and P. Beynon, *Chem. Phys. Lipids*, 1973, **10**, 37.
16 E. Oldfield, D. Chapman and W. Derbyshire, *FEBS Lett.*, 1971, **16**, 102.
17 E. Oldfield, D.Chapman and W. Derbyshire, *Chem. Phys. Lipids*, 1972, **9**, 69.
18 R. L. Smith and E. Oldfield, *Science*, 1984, **225**, 280.
19 E. Oldfield, J. L. Bowers and J. Forbes, *Biochemistry*, 1987, **26**, 6919.
20 J. Forbes, C. Husted and E. Oldfield, *J. Am. Chem. Soc.*, 1988, **110**, 1059.
21 R. A. Haberkorn, J. Herzfeld and R. G. Griffin, *J. Am. Chem. Soc.*, 1978, **100**, 1296.
22 M. D. Sefcik, J. Schaefer, E. O. Stejskal, R. A. McKay, J. F. Ellena, S. W. Dodd and M. F. Brown, *Biochim. Biophys. Res. Commun.*, 1983, **114**, 1048.
23 J. W. de Haan, R. J. E. M. de Weerd, L. J. M. van de Ven, F. A. H. den Otter and H. M. Buck, *J. Phys. Chem.*, 1985, **89**, 5518.
24 J. R. Brainard and E. H. Cordes, *Biochemistry*, 1981, **20**, 4607.
25 D. Abramson and M. Blecher, *J. Lipid Res.*, 1964, **5**, 628.
26 J. C. Dittmer and R. L. Lester, *J. Lipid Res.*, 1964, **5**, 126.
27 W. T. Norton, *Methods in Enzymology*, ed. S. Fleisher and L. Packer (Academic Press, New York, 1974), vol. 31, pp. 435–444; M. Moscarello, unpublished results.
28 M. M. Maricq and J. S. Waugh, *J. Chem. Phys.*, 1979, **70**, 3300.
29 J. P. Yesinowski and M. J. Mobley, *J. Am. Chem. Soc.*, 1983, **105**, 6191.
30 K. D. Lawson and T. J. Flautt, *J. Phys. Chem.*, 1968, **72**, 2066.
31 H. Wennerström, *Chem. Phys. Lett.*, 1973, **18**, 41.
32 M. Bloom, E. E. Burnell, S. B.W. Roeder and M. I. Valic, *J. Chem. Phys.*, 1977, **66**, 3012.
33 M. Bloom, E. E. Burnell, A. L. MacKay, C. P. Nichol, M. I. Valic and G. Weeks, *Biochemistry*, 1978, **17**, 5750.
34 N. J. M. Birdsall, J. Feeney, A. G. Lee, Y. K. Levine and J. C. Metcalfe, *J. Chem. Soc., Perkin Trans. 2*, 1972, 1441.
35 E. R. Andrew, *J. Chem. Phys.*, 1950, **18**, 607.
36 E. Oldfield, M. Meadows, D. Rice and R. Jacobs, *Biochemistry*, 1978, **17**, 2727.
37 H-U. Gally, W. Niederberger and J. Seelig, *Biochemistry*, 1975, **14**, 3647.
38 P. R. Cullis and B. de Kruyff, *Biochim. Biophys. Acta*, 1976, **436**, 523.
39 B. Schneider, J. Spevacek, N. X. Phuc., *Acta Phys. Pol. A*, 1985, **68**, 841.
40 R. Teeäär, M. Alla and E. Lippmaa, *Org. Magn. Reson.*, 1982, **19**, 134.
41 J. Forbes and E. Oldfield, unpublished results.
42 A. Darke, E. G. Finer, A. G. Flook and M. C. Phillips, *FEBS Lett.*, 1971, **18**, 326.
43 P. A. Kroon, M. Kainosho and S. I. Chan, *Nature (London)*, 1975, **256**, 582.
44 S. A. Penkett, A. G. Flook and D. Chapman, *Chem. Phys. Lipids*, 1968, **2**, 273.

45 N. J. M. Birdsall, A. G. Lee, Y. K. Levine and J. C. Metcalfe, *J. Chem. Soc., Chem. Commun.*, 1971, 1171.
46 A. F. Horwitz, W. J. Horsley and M. P. Klein, *Proc. Natl Acad. Sci. USA*, 1972, **69**, 590.
47 Z-C. Xu and D. S. Cafiso, *Biophys. J.*, 1986, **49**, 779.
48 N. E. Gabriel and M. F. Roberts, *Biochemistry*, 1987, **26**, 2432.
49 J. E. Anderson and W. P. Slichter, *J. Phys. Chem.*, 1965, **69**, 3099.
50 D. C. Douglass and G. P. Jones, *J. Chem. Phys.*, 1966, **45**, 956.
51 M. J. Ruocco, D. Atkinson, D. M. Small, R. P. Skarjune, E. Oldfield and G. G. Shipley, *Biochemistry*, 1981, **21**, 5957.
52 A. Seelig and J. Seelig, *Biochemistry*, 1974, **13**, 4839.
53 M. Mathlouthi, A. L. Cholli and J. L. Koenig, *Carbohydr. Res.*, 1986, **147**, 1.
54 B. D. Ladbrooke and D. Chapman, *Chem. Phys. Lipids*, 1969, **3**, 304.
55 H. J. Reich, M. Jautelat, M. T. Messe, F. J. Weigert and J. D. Roberts, *J. Am. Chem. Soc.*, 1969, **91**, 7445; J. W. ApSimon, J. Beierbeck and J. K. Saunders, *Can. J. Chem.*, 1973, **51**, 3874.
56 A. Pines, M. G. Gibby and J. S. Waugh, *J. Chem. Phys.*, 1972, **56**, 1776.
57 E. C. Williams and E. H. Cordes, *Biochemistry*, 1976, **15**, 5792.
58 W. T. Norton and W. Cammer, in *Myelin*, ed. P. Morell (Plenum Press, New York, 2nd edn, 1984), pp. 147–195.
59 J. Dabrowski, H. Egge and P. Hanfland, *Chem. Phys. Lipids*, 1980, **26**, 187.
60 H. L. Holland, P. R. P. Diakow and G. J. Taylor, *Can. J. Chem.*, 1978, **56**, 3121.
61 P. Joseph-Nathan, G. Mejía and D. Abramo-Bruno, *J. Am. Chem. Soc.*, 1979, **101**, 1289.
62 S. A. Knight, *Org. Magn. Reson.*, 1974, **6**, 603.
63 J. G. Batchelor, R. J. Cushley and J. H. Prestegard, *J. Org. Chem.*, 1974, **39**, 1698.
64 L. O. Sillerud, C. H. Han, M. W. Bitensky and A. A. Francendese, *J. Biol. Chem.*, 1986, **261**, 4380.
65 R. Murari, M. M. A. Abd El-Rahman, Y. Wedmid, S. Parthasarathy and W. J. Baumann, *J. Org. Chem.*, 1982, **47**, 2158.

Paper 8/00812D; *Received 29th February*, 1988